โครงการ
การเรียนการสอนเพื่อเสริมประสบการณ์

ชื่อโครงการ   ผลของการไหลแบบเฉือนที่เหนี่ยวนำให้เกิดรูเปิดซึ่งมีผลต่อการกรองของโกลเมอรูลัสและการคัดเลือกสารโดยใช้ขนาด

Effects of shear flow-Induced opening on glomerular filtration and size-selectivity

ชื่อนิสิต   นายฐาปกรณ์ แพนเกาะ   **เลขประจำตัว**   5933419023

ภาควิชา   ฟิสิกส์
ปีการศึกษา   2562

คณะวิทยาศาสตร์ จุฬาลงกรณ์มหาวิทยาลัย

Project tittle   Effects of shear flow-induced openings on glomerular fluid filtration and size-selectivity

Author   Mr.Thapakorn Pankoh ID 5933419023

Project advisor   Asst. Prof. Panadda Dechadilok (Ph.D)

Department   Physics

Academic year   2019

Accepted by the Department of Physics, Faculty of Science, Chulalongkorn University in partial fulfillment of the Requirements for the bachel. r's degree

THESIS COMMITTEE

…………………………………………..

Dr.Santipong Boribarn

(Chairman of the examination committee)

…………………………………………..

Dr.Yuttana Roongthumskul

(Examination committee)

…………………………………………..

Asst.Prof.Dr.Panadda Dechadilok

(Advisor / Examination committee)

Project tittle	Effects of shear flow-induced openings on glomerular fluid filtration and size-selectivity
Author	Mr.Thapakorn Pankoh ID 5933419023
Project advisor	Asst. Prof. Panadda Dechadilok (Ph.D)
Department	Physics
Academic year	2019

Abstract

Kidneys are vital organs of which main function is to maintain constant blood volume and composition by removing excess fluid and metabolic waste from the circulation through urine formation. It is believed that the first step of renal urine formation is the filtration of fluid and solutes through the glomerular barrier with its unique nanostructure. Two-third of the glomerular capillary surface area consists of three cellular layers, a filtration slit connected to epithelial foot processes, an associated area of glomerular basement membrane (GBM) and several endothelial fenestrae, commonly referred to as the filtration surface, whereas one-third of the glomerular capillary surface is a four-layered barrier with the glomerular mesangium located between the endothelial cell layer and GBM. A comparison between the mathematical model employing hindered transport theory and the ficoll sieving coefficient obtained from *in vivo* urinanalysis has shown that the assumption of the fluid and solute fluxes flowing through the intact glomerular barrier, although capable of explaining filtration of small and medium-sized solutes, greatly underestimates the sieving coefficient of solutes with the radius larger than 5 nm. In addition, it also contradicts with the fact that, even in normal humans, a small amount of red blood cells is observed in urine. Electron micrographs have shown red blood cells "escaping" through the small openings at the junction where the three-layered filtration surface meets the four-layered barrier. In the present work, the effects of these openings on the glomerular fluid and solute filtration are investigated using low-Reynolds-number fluid dynamics and hindered transport theory. Although their effects on the overall glomerular hydraulic permeability and the filtration of small and medium-sized solutes are found to be small, the presence of the possibly shear-induced openings greatly increases the sieving coefficient of large solutes, rendering the calculated sieving coefficients that agree well with the ficoll sieving coefficients obtained from experiments performed in normal humans and patients with diabetic nephropathy for the entire range of solute size.

Acknowledgement

The thankful of this project is consist of my parts. First, I would like to express my sincere gratitude to my advisor, Asst.Prof.Dr.Panadda Dechadilok who always teach and support me for many things that I do not understand. Next, I would like to thank for both committees, Dr.Santipong Boribarn and Dr.Yuttana Roongthumskul for their guidance to this project. In addition, I am grateful to Assoc.Prof.Pisut Katavetin, MD for suggestions and all his help. I am gratefully acknowledged for the opportunity to create this project from Department of Physics, Faculty of Science, Chulalongkorn University. Finally, I would like thank to Mr.Numpong Punyaratabandhu for his support.

Thapakorn Pankoh

Contents

List of Figures

List of Tables

Chapter 1

Introduction

1.1) Motivation

Kidneys, organs on either side of the spine in the posterior abdominal wall, are protected by muscle, fat, and ribs [1]. Its primary function is to maintain constant composition and volume of blood plasma in circulation by removing excess fluid and metabolic waste through renal urine formulation [2]. The first step of this process is blood ultrafiltration where blood from the intravascular space is filtered through glomerular capillary wall and becomes a primary urine in Bowman's space [3]. Normally, the glomerular barrier allows smalls solute to pass into primary while retaining large macromolecules such as proteins and blood cells.

The glomerular barrier structure is shown schematically in Fig. 1. The barrier is often categorized into two components; the filtration surface consisting of three cellular layers that are the fenestrated endothelial cell layer, glomerular basement membrane (GBM) and the epithelial cell layer, and the four layered barrier that includes the mesangium between the endothelium and GBM.
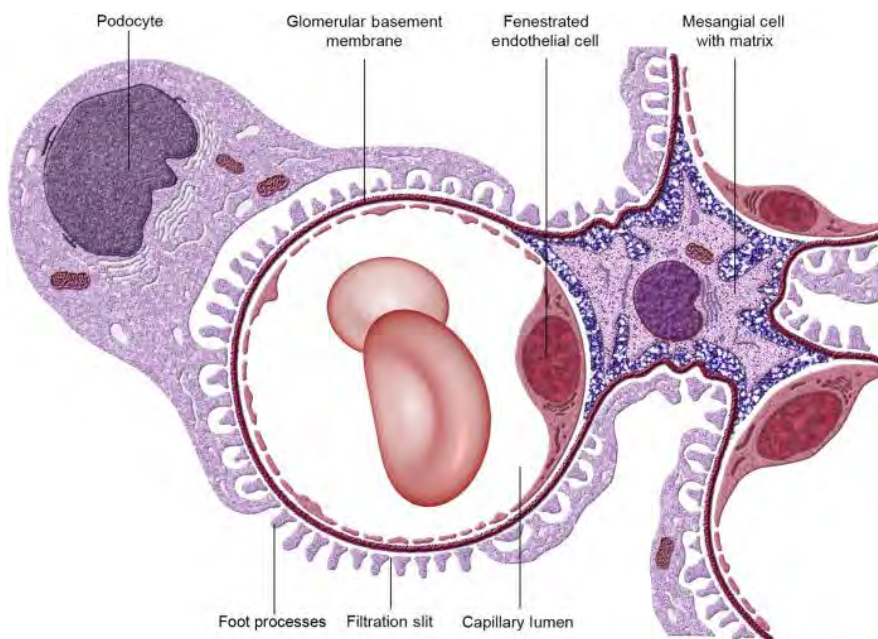
Fig. 1 The glomerular filtration structures. The barrier categorized two components; the filtration surface with 3 layers that are the fenestrated endothelial cell layer, glomerular basement membrane (GBM) and the epithelial cell layer, and the four layered barrier that includes the mesangium between the endothelium and GBM. [4]

At the glomerular intravascular pressure above 58 mmHg (possible with patients with hypertension), transient short-lived transcellular and intracellular openings are observed at the endothelial cell layers [5,6]. Experimental evidences include electron microscopic images displaying red blood cells (RBC) escaped from the capillary lumen into Bowman's space (show in Fig. 2), indicating hematuria, symptom where blood cells are detected in urine's patients [7]. The "openings" large enough for RBC passages are often observed at the jointed area between the filtration surface and the mesangium as shown in Figs. 3A- 3C. In the present work, it is speculated that the occurrence of these openings might be due to the more uniform orientation of type IV collagens induced by the shear flow, resulting in the reduction of the ability of GBM to withstand pressure and hydrodynamic flow. This speculation is based on an

experimental study reporting that the increase in the volume flow rate of a shear flow correlates with the decrease in the standard deviation in the orientation of type I collagens in microfluidic channels. In addition, it is worth noting the maximum fluid velocity gradient is observed at the jointed area between the filtration surface and the mesangium. The objective of this project is to investigate the contribution of the glomerular barrier openings on the glomerular hydraulic permeability (estimated from the glomerular filtration rate (GFR)) as well as the contribution to size-selectivity (measured as solute sieving coefficient: the ratio between the solute concentration in the primary urine in Bowman's space and that in the plasma.
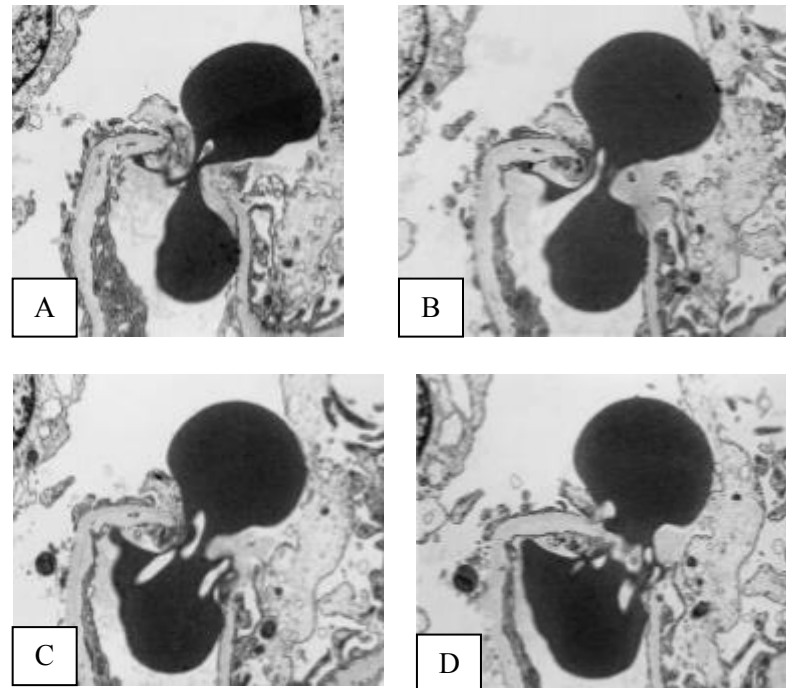
Fig. 2 The serial cross section shows a red blood cell transversing from intravascular to Bowman's space (A-D). [8]

1.2) Project objective

(1) Determine the fluid volume flow rate through shear flow-induced glomerular barrier opening
(2) Determine the effect of these opening on glomerular size-selectivity and the change in the sieving coefficient of ficolls (highly cross-linked polysaccharides behaving like a rigid hydrodynamic spherical particle).

1.3) Definitions of variables and parameters

L : pore length

R : radius of pore

R_0 : maximum pore radius

v : fluid velocity

ρ : fluid density

$\wp$: fluid dynamic pressure

μ : shear viscosity, plasma viscosity

Re   : Reynold number

f_T : dimensionless flow resistance

k_{3layer} : hydraulic permeability through glomerular filtration surface

k_{4layer} : hydraulic permeability through glomerular mesangium

N   : the number of pores and solute flux

R_v : volume floe rate

τ : time of period

r_s : solute radius

U   : solute molecule velocity

C   : solute concentration

k   : Boltzmann's constant

D_∞ : diffusivity in dilute bulk solution

T   : Temperature

β : dimensionless radial position of solute particle

λ : ratio of solute radius and pore radius

E   : potential of long-range interaction

K_d : hindrance factor of diffusion

K_c : hindrance factor of convection

Φ : partition coefficient

Pe   : Peclet number

θ : sieving coefficient

S_{3layer} : glomerular filtration surface area

S_{4layer} : glomerular mesangium surface area

Chapter 2

Model Development

In this work, we assume that the solute is a rigid uncharged spherical particle large enough to be viewed as a hydrodynamic particle with the no-slip boundary condition applicable at its surface. The requirement is that it must be at least several times larger than the solvent molecule. The solution is dilute such that solute-solute interaction is negligible. The shear-induced opening observed at the jointed area between the three-layered filtration surface and the four-layered that includes the mesangium (shown schematically in Figs. 3A and 3B) is assumed to be a circular pore. Its length (L) equals the GBM thickness; in patients with diabetic nephropathy, L is approximately 800 nm, whereas in healthy human, it is estimated to be 400 nm. As shown in Fig. 3C, R is the radius of the shear-induced opening that varies as a function of time. Its maximum value (R_0) is estimated from an electron micrograph [8] to be 80 nm. The flow is assumed to be mainly in the z-direction. The estimated Reynolds number is found to be small enabling one to find the fluid velocity and pressure by solving Stokes' equation. In Sec 2.1, the calculation of the dimensionless flow resistance is presented, whereas in Sec. 2.2, the computation of the hydrodynamic pressure from single nephron glomerular filtration rate (SNGFR) is discussed.
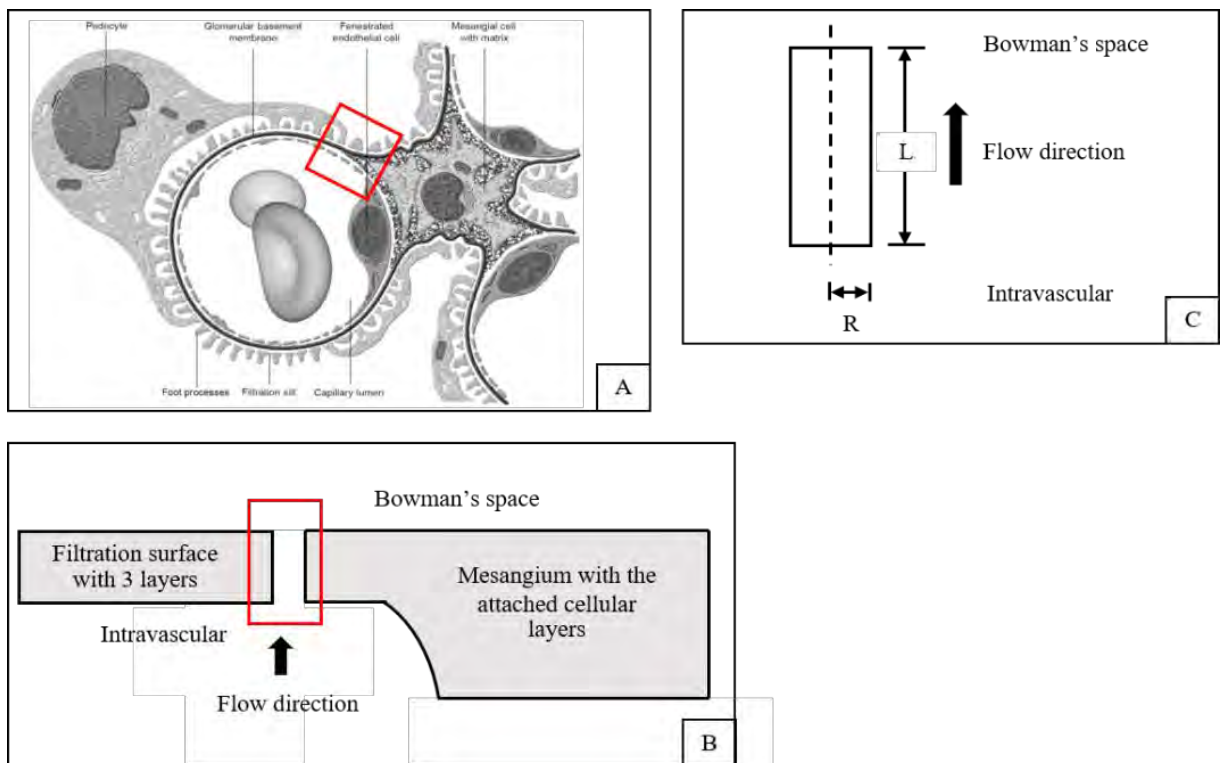
Fig. 3 (A) Schematic drawing of the glomerular capillary cross-section. Indicated in the figure (as the red block) is the area where the "opening" or the temporary "pore" is most often observed. (B) Simplified geometry of the pore, the filtration surface and the glomerular mesangium with the attached cellular layers. (C) Schematic drawing of the shear-induced opening or pore.

2.1) Dimensionless flow resistance for a creeping flow in a cylindrical pore as a function of the ratio between its length and its radius

The fluid velocity and pressure of an incompressible Newtonian fluid is generally computed as a solution of the Navier-Stokes equation [20]:

$$\rho\left(\frac{\partial \vec{v}}{\partial t} + \vec{v}.\vec{\nabla}\vec{v}\right) = -\vec{\nabla}\wp + \mu\nabla^2\vec{v} \qquad (1)$$

where $\vec{v}$ is the fluid velocity and $\wp$ is the fluid dynamic pressure, whereas μ is the shear viscosity and ρ is the fluid density. Eq. (1) is essentially Newton's second law in the form that is appropriate for fluid motion. The terms on left-hand side contains the "material derivate" of a linear momentum (per volume) whereas the terms on the right-hand side originates from the forces (which are pressure and viscous dissipation). The first term on the left-hand side is simply the change in momentum, whereas the second term is the inertia term sometimes viewed as convection of momentum. Convective term tends to be prominent when Re>>1 and nearly absent when Re<<1 [9,10]. For a steady flow with the Reynolds number being much smaller than 1, all the terms on the left-hand side are negligible, resulting in the Navier-Stokes equation being linearized as [20]

$$0 = -\vec{\nabla}\wp + \mu\nabla^2\vec{v} \qquad (2)$$

Equation (2) is Stokes' equation which must be solved at the same time with the continuity equation (corresponding to a conservation of mass) expressed as follows. [20]

$$\frac{\partial \rho}{\partial t} + \vec{\nabla}\bullet\left(\rho\vec{v}\right) = 0 \qquad (3)$$

For an incompressible fluid, ρ is constant, resulting in the following form of the continuity equation.

$$\vec{\nabla}\bullet\vec{v} = 0 \qquad (4)$$

Equations (2) and (4) must be solved together as coupled differential equations in order to determine the fluid velocity, and pressure. For the system of our interest, the fluid velocity must satisfy the no-slip boundary condition at the "pore surface";

$$\left|\vec{v}\right| = v_{3\,layer} = k_{3\,layer}\,\Delta\wp \qquad (5)$$

where $k_{3\,layer}$ is the hydraulic permeability of the three-layered glomerular filtration surface and $\Delta\wp$ is the hydrodynamic pressure difference across the glomerular filtration surface. In other words, at the interface between the shear-induced opening and the glomerular filtration surface, the fluid velocity is assumed to be equivalent to the averaged velocity of a fluid filtrating through the glomerular basement membrane ($v_{3\,layer}$). Because Stokes' equation is linear, its solution can be expressed as a superposition of solutions as follows.

$$v_z = v_z^{(1)} + v_z^{(2)} \tag{6}$$

where $v_z^{(1)}$ is the solution of the Stokes and continuity equations that satisfy the homogenous no-slip boundary condition of a stationary pore wall; $v_z^{(1)} = 0$ at the pore wall. In the present work, $v_z^{(1)}$ is obtained as a finite element solution (COMSOL Multiphysics). $v_z^{(2)}$, on the other hand, is $v_{3\,layer}\,\bar{e}_z$. As it is a constant, it automatically satisfies Eqs. (2) and (4) as well as the inhomogeneous boundary condition stated in Eq. (5).

It is worth noting that, for a pore with L at least 10 times larger than R, the pore entrance effect on the fluid motion is negligible, and the flow can be considered as a unidirectional fully developed flow where Eq. (2) can be written as

$$0 = -\frac{\partial\wp}{\partial z} + \mu\left(\frac{1}{r}\frac{\partial}{\partial r}\left(r\frac{\partial v_z^{(1)}}{\partial r}\right)\right) \tag{7}$$

The solution of Eq. (7) can be obtained analytically; it is the velocity of a Poiseuille flow in a circular tube:

$$v_z^{(1)} = -\frac{1}{\mu}\frac{\partial\wp}{\partial z}\left(\frac{R^2}{4}\right)\left(1-\left(\frac{r}{R}\right)^2\right) \tag{8}$$

$v_z^{(1)}$ is then averaged over all the opening cross-section as the velocity can be calculated, as shown below.

$$\left\langle v_z^{(1)}\right\rangle = \frac{1}{\pi R^2}\int_0^{2\pi}\int_0^R v_z^{(1)}\,r\,dr\,d\theta \tag{9}$$

By completing the integration in Eq. (10), one obtains

$$\left\langle v_z^{(1)}\right\rangle = -\frac{1}{8\mu}\left(\frac{\partial\wp}{\partial z}\right)R^2 \tag{10}$$

where $\dfrac{\partial \wp}{\partial z}$ is a constant; $\dfrac{\partial \wp}{\partial z} = \dfrac{\Delta \wp}{L}$.

In the field of fluid mechanics, the pore resistance of fluid flow is often expressed in terms of the dimensionless flow resistance (f_T), a pressure difference required in overcoming a unit of viscous stress. For the Poiseuille flow in a long cylindrical pore, f_T is expressed as

$$f_T = \frac{\Delta \wp}{\mu \left\langle v_z^{(1)} \right\rangle / R} \qquad (11)$$

Substituting Eq. (10) in Eq. (11), the dimensionless flow resistance is simply

$$f_T = \frac{8 L}{R} \qquad (12)$$

As shown in Figs. 4 and 5, f_T of a creeping flow in a cylindrical pore obtained by using finite element method is compared to an analytical result stated in Eq. (12). Although the dimensionless flow resistance expressed in Eq. (12) is strictly valid for a pore with $L \gg R$, we found that this expression yields results with less than 2% error for $L \geq 5R$. As discussed earlier, for healthy human, $L = 400 \, \text{nm} = 5R_0$, whereas, in the case of patients with diabetic nephropathy, L is likely to be even larger. Eq. (12), is, therefore employed in the calculation of f_T.
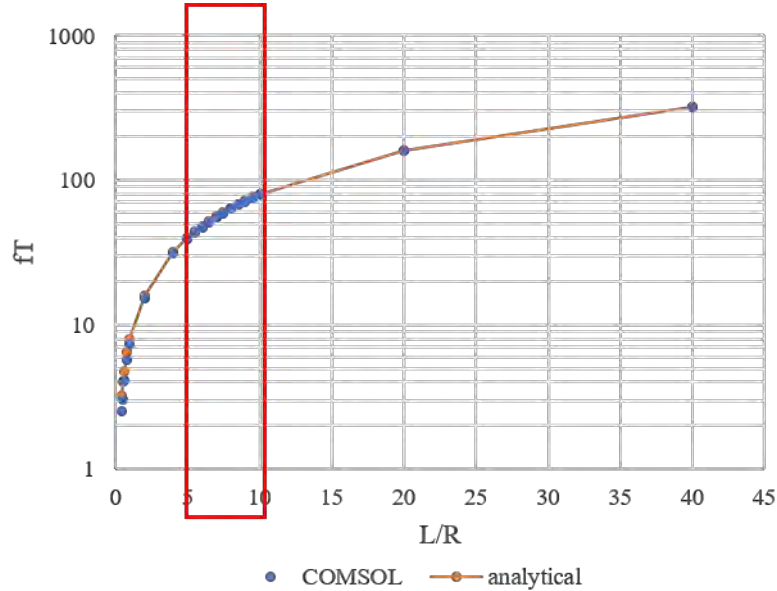
Fig. 4 The dimensionless flow resistance for a creeping flow in a cylindrical pore (f_T) calculated analytically and that obtained as a finite element solution as a function of the ratio between the pore length and pore radius (L / R).
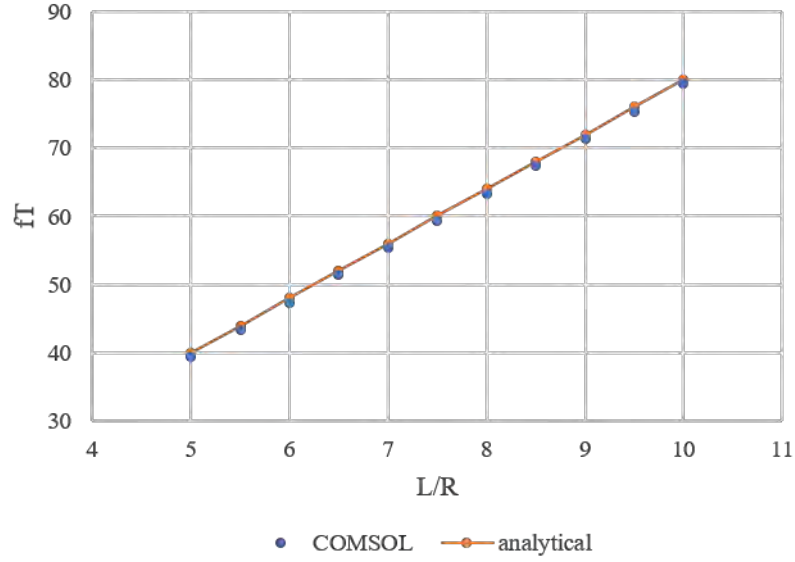
Fig. 5 Close inspection of dimensionless flow resistance for a creeping flow in a cylindrical pore (f_T) calculated analytically and that obtained as a finite element solution with L/R being in the range of 5 - 10.

2.2) The average volume flow rate of a creeping flow through a pore with radius varying as a function of time

The averaged fluid velocity through the pore described in Sec. 2.1 is an addition of the averaged values of $v_z^{(1)}$ and $v_z^{(2)}$ as follows.

$$\langle v_z \rangle = \langle v_z^{(1)} \rangle + \langle v_z^{(2)} \rangle \tag{13}$$

where, according to Eq. (11), the averaged value of $v_z^{(1)}$ can be expressed as

$$\langle v_z^{(1)} \rangle = f_T^{-1} \left(R / \mu \right) \Delta P . \tag{14}$$

As discussed earlier, $v_z^{(2)}$ is constant, and therefore, so is its averaged value;

$$\langle v_z^{(2)} \rangle = v_z^{(2)} = k_{3\,layer} \Delta \wp . \tag{15}$$

It has been speculated that the shear-induced opening at the junction between the filtration surface and the glomerular mesangium opens and closes periodically because, if such pores open all the time, hematuria is likely to be unavoidable. If the period during which these pores remain open is τ and the

number of shear-induced opening per glomerulus is N, the volume flow rate averaged over the pore cross-section can be computed as

$$\langle R_v \rangle_{pore} = \frac{N}{\tau} \int_0^\tau \left(\pi R^2 \right) \langle v_z \rangle \, dt \, .$$

(16)

Substituting the expressions in Eq. (14) and (15) into Eq. (16), one obtains the following expression.

$$\langle R_v \rangle_{pore} = \frac{N \pi \Delta \wp}{\tau} \int_0^\tau \left(\frac{R^4}{8\mu L} + k_{3\,layer} R^2 \right) dt$$

(17)

where R, the radius of the pore, is a function of time. We consider two possible options for $R(t)$. If the opening and closing of pore happens slowly, $R(t)$ can be viewed as a sine function as follows.

$$R(t) = R_0 \sin\left(\frac{\pi t}{\tau} \right)$$

(18)

The second option is that, if the GBM rupture is sudden but the closing of the pore is slow (as it requires a formation of vesicles), $R(t)$ can be viewed as a cosine function as shown below.

$$R(t) = R_0 \cos\left(\frac{\pi t}{2\tau} \right)$$

(19)

For both options for $R(t)$, however, the average of the volume flow rate turns out to be exactly the same as shown below. (details show in Appendix D)

$$\langle R_v \rangle_{pore} = N \pi \Delta \wp \left[\frac{3}{64} \frac{R_0^4}{\mu L} + \frac{1}{2} k_{3\,layer} R_0^2 \right]$$

(20)

Equation (20) also allows us to investigate the effect of $\langle R_v \rangle_{pore}$ on the hydrodynamic pressure difference $\left(\Delta \wp \right)$ and single nephron glomerular filtration rate (SNGFR), the volume flow rate per glomerulus. As discussed in details in Appendix A, the effect of $\langle R_v \rangle_{pore}$ on both factors is less than 1% if N < 30. In our calculation, $\Delta \wp$ and SNGFR are assumed to be similar to those previously employed in the calculation in absence of the shear-induced openings. The effect of the presence of the shear-induced pore openings on the glomerular size-selectivity is discussed further in the next section.

2.3) The average solute flux carried by a creeping flow through a cylindrical pore: Faxen's first law

In order to examine the effects of the fluid flow through the shear-induced openings at the junction where the filtration surface meets the glomerular mesangium on the solute sieving, the ratio between the solute concentration in the primary urine in Bowman's space and that in the capillary lumen, a mathematical model employing hindered transport theory is developed. As aforementioned, in this model, the solutes are assumed to be at least several times larger than the solvent molecules such that they can be viewed as Brownian particles suspended in a continuum medium (that is the fluid solvent). The solution is assumed to be dilute such that effects of solute-solute interaction is negligible. Because the solute radius (r_s) of ficolls from *in vivo* urinanalysis are in the range of $1.6 - 6$ nm and are much smaller than the pore radius (R) and the Reynolds number characterizing the flow is very small, the hydrodynamic drag is calculated using Faxen's first law as follows [9].

$$F = -6\pi\mu r_s \left[\left(\vec{U} - \vec{v}\right) - \frac{r_s^2}{6}\left(\nabla^2 \vec{v}\right) \right] \qquad (21)$$

The solute motion, under the assumption that it is steady and happens in an isothermal fluid, is governed by the balance between the chemical potential gradient (viewed as a body force acted on the solute molecule [11]) and the hydrodynamic drag the fluid solvent exerted on the solute as shown below.

$$-kT\nabla\ln C - 6\pi\mu r_s \left[\left(\vec{U} - \vec{v}\right) - \frac{r_s^2}{6}\left(\nabla^2 \vec{v}\right) \right] = 0 \qquad (22)$$

where k is Boltzmann's constant and T is the temperature. C is the solute concentration, and μ is the solvent viscosity. $\vec{U}$ and $\vec{v}$ are the velocity of the solute molecule and that of the unperturbed fluid, respectively. The first term of Eq.(22) represents the chemical potential gradient in the, whereas the second and third terms (in the bracket) correspond to the drag force according to Faxen's first law. A rearrangement of Eq. (22) leads to the following expression.

$$U = -D_\infty \nabla\ln C + \vec{v} + \frac{r_s^2}{6}\left(\nabla^2 \vec{v}\right) \qquad (23)$$

where D_∞ is the solute diffusivity in a dilute bulk solution defined as

$$D_\infty = \frac{kT}{6\pi\mu r_s}. \qquad (24)$$

The solute flux is given by $\vec{N} = \vec{U}C$. According to Eq. (23), it can be written as

$$\vec{N} = -D_\infty \nabla C + \vec{v}C + \frac{r_s^2}{6}C\left(\nabla^2 \vec{v}\right)$$ (23)

Next, a solute molecule confined in a shear-induced opening (at the junction between the filtration surface and the glomerular mesangium) is considered. As shown in Fig. 6, the dimensionless distance from the pore centerline to the solute center is denoted as β which is the ratio between the radial location of the particle center (r) and pore radius; $\beta = r/R$. It is clear that $0 \le \beta \le 1$. Because the approximated shape of the test solutes used in the experiments, ficolls, is that of a sphere, in our calculation, the solute is assumed to be spherical. The relative size of the solute is denoted as λ; $\lambda = r_s/R$.

$$C(z=0) = C_0 \qquad C(z=0) = \Phi C_0 \qquad C(z=L) = \Phi C_L \qquad C(z=L) = C_L$$

$$z = 0 \qquad \lambda = r_s/R \qquad L \qquad \beta = r/R \qquad z = L$$
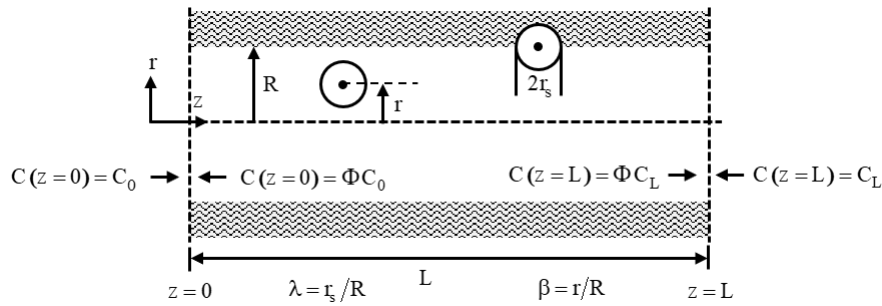
Fig. 6 A schematic drawing of a spherical solute confined in a cylindrical pore with the pore wall being a loose fibrous membrane. R is the pore radius and L is the pore length, whereas, r_s is the solute radius.

As aforementioned, the average fluid velocity in the shear-induced opening is the summation of average velocity of a Poiseuille flow and the velocity at pore surface. According to Eqs. (13) – (15), the glomerular hydrodynamic pressure difference can be expressed as a function of the averaged fluid velocity as follows.

$$\Delta \wp = \frac{\langle v_z \rangle}{\left(\dfrac{R^2}{8\mu L} + k_{3\,layer}\right)}$$ (24)

Substituting the expression in Eq. (26) into Eqs. (13) – (15), one obtains the fluid velocity at a given radial location inside the pore as a function of the averaged velocity as shown below.

$$\vec{v} = 2\langle v_z \rangle \left[\frac{R^2\left(1-\beta^2\right) + 4\mu L k_{3\,layer}}{R^2 + 8\mu L k_{3\,layer}}\right] \vec{e}_z$$ (25)

The Laplacian of the fluid velocity is, therefore

$$\nabla^2 \vec{v} = \frac{-8\langle \vec{v}_z \rangle}{R^2 + 8\mu L k_{3\,layer}}$$

(26)

Eq. (27) and (28) allow one to obtain an expression for a more useful quantity that is related to the measurable sieving coefficient, the solute flux averaged over the pore cross-section $\left(\langle \overline{N} \rangle \right)$, defined as

$$\langle \vec{N} \rangle = \frac{\int\limits_{0}^{2\pi} \int\limits_{0}^{1} \overline{N}\beta\, d\beta\, d\phi}{\int\limits_{0}^{2\pi} \int\limits_{0}^{1} \beta\, d\beta\, d\phi} = 2\int\limits_{0}^{1} \overline{N}\beta\, d\beta$$

(27)

If L >> R, the solute concentration can be expressed as a product of a function of axial position and that of a radial position inside the pore as [11]

$$C = g(z)\exp\left(-E(\beta)/kT\right)$$

(28)

where E is a potential energy of interaction associated with the long range interaction between solute molecule and the pore surface. The solute concentration averaged over the pore cross-section is

$$\langle C \rangle = \frac{\int\limits_{0}^{2\pi} \int\limits_{0}^{1} C\beta\, d\beta\, d\phi}{\int\limits_{0}^{2\pi} \int\limits_{0}^{1} \beta\, d\beta\, d\phi} = 2\int\limits_{0}^{1} C\beta\, d\beta$$

(29)

where its derivative can be expressed as follows.

$$\frac{\partial \langle C \rangle}{\partial z} = 2\int\limits_{0}^{1} \frac{\partial C}{\partial z}\beta\, d\beta$$

(30)

In addition, $\langle \vec{N} \rangle = \langle N \rangle \vec{e}_z$. Substitutions of expressions in Eqs.(23), (25), (26), (29) and (30) into Eq.(27) yield the following expression for the cross-sectional averaged fluid flux.

$$\langle N \rangle = -D_\infty \frac{\partial \langle C \rangle}{\partial z} + \frac{2\langle v \rangle \langle C \rangle R^2}{R^2 + 8\mu L k_{3\,layer}}\left[\gamma + \frac{4\mu L k_{3\,layer}}{R^2} - \frac{2}{3}\left(\frac{r_s}{R}\right)^2 \right]$$

(31)

where

$$\gamma = \frac{\int\limits_0^1 \left(1-\beta^2\right)\exp\left(-E(\beta)/kT\right)\beta\,d\beta}{\int\limits_0^1 \exp\left(-E(\beta)/kT\right)\beta\,d\beta} \tag{32}$$

Once E is determined, it would be possible to calculate the cross-sectional averaged solute flux and, subsequently, the solute sieving coefficient.

2.4) The convective hindrance factor of a sphere confined in a cylindrical pore

In this work, as 90% of GBM volume is that of fluid and only 10% is the total volume of the fibers, we assume the solute molecule and pore surface (mainly GBM surface) are not interacting (since the percentage of the fiber volume fraction is quite low), and that implies that E = 0 (in an approximate sense). γ, therefore, becomes

$$\gamma = \frac{\int\limits_0^1 \left(1-\beta^2\right)\beta\,d\beta}{\int\limits_0^1 \beta\,d\beta} = \frac{1}{2} \tag{33}$$

The axial component of average total solute flux can be re-written as [12]

$$\langle N \rangle = -K_d D_\infty \frac{\partial \langle C \rangle}{\partial z} + K_c \langle v_z \rangle \langle C \rangle \tag{36}$$

where K_d and K_c are diffusive and convective hindrance factors, respectively. K_d is the ratio between the intrapore solute diffusivity and those in the external bulk solution. K_c, on the other hand, is the ratio between the cross-sectional averaged convective solute flux and $\langle v_z \rangle \langle C \rangle$; it indicates how the hydrodynamic interaction changes the rate of solute convection. By comparing the coefficients of the term on the right hand side of Eq. (36) to those of Eq.(33), we found that $K_d = 1$, whereas the convective hindrance factor, K_c, can be expressed as

$$K_c = \frac{2R^2}{R^2 + 8\mu L k_{3\,layer}} \left[\frac{1}{2} + \frac{4\mu L k_{3\,layer}}{R^2} - \frac{2}{3}\left(\frac{r_s}{R}\right)^2\right] = 1 - \frac{4}{3}\frac{r_s^2}{R^2 + 8\mu L k_{3\,layer}} \tag{37}$$

Assuming that the flux is conserved, Eq.(36) can be rearranged in a form involving integrands as

$$\int_{z=0}^{z=L} -\frac{1}{K_d D_\infty}\,dz = \int_{C(z=0)}^{C(z=L)} \frac{1}{\langle N\rangle - K_c \langle v\rangle \langle C\rangle}\,d\langle C\rangle \tag{38}$$

where $C(z = 0)$ and $C(z = L)$ are the upstream and downstream solute concentrations inside the cylindrical pore; as shown in Fig. 6, assuming equilibrium, they are equal to the adjacent external solute concentration multiplied by equilibrium partition coefficient Φ [12]. $C(z=0)=\Phi C_0$ and $C(z=L)=\Phi C_L$ where C_0 and C_L are the external upstream and downstream solute concentration, respectively. An integration of Eq. (38) yields

$$\langle N\rangle = \Phi K_c \langle v\rangle C_0 \frac{\left[1-\left(C_L/C_0\right)e^{-Pe}\right]}{1-e^{-Pe}} \tag{39}$$

where Pe is the Peclet number, a dimensionless parameter indicating the relative importance of convection and diffusion, defined as

$$Pe = \frac{\Phi K_c \langle v\rangle L}{\Phi K_d D_\infty} \tag{40}$$

If Pe $\ll$ 1, diffusion dominates, whereas, if Pe $\gg$ 1, convection is the dominant process. As Bowman's space is viewed as a dead end chamber, the downstream solute concentration is determined from the ratio of the solute flux divided by average fluid velocity; $C_L = \langle N\rangle/\langle v\rangle$ [12]. Substituting this expression for C_L into Eq. (39), the cross-sectional average flux can be written as

$$\langle N\rangle = \frac{\Phi K_c \langle v\rangle C_0}{1-\left(1-\Phi K_c\right)e^{-Pe}} \tag{41}$$

Typically, the partition coefficient (if the solute and the pore are both uncharged and the interaction is purely steric) is the fraction of the intrapore radial positions accessible for the solute. As we are assuming that all radial positions is available for the sphere center, $\Phi = 1$. In addition, $K_d = 1$. Eq. (41) becomes simplified as

$$\langle N\rangle = \frac{K_c \langle v\rangle C_0}{1-\left(1-K_c\right)e^{-Pe}} \tag{42}$$

where

$$Pe = \frac{K_c \langle v\rangle L}{D_\infty}. \tag{43}$$

The next step is to relate the cross-sectional averaged flux to the measurable solute sieving coefficient as will be discussed in the next section.

2.5) Calculation of sieving coefficient

2.5.1) Calculation of the sieving coefficient of a solute confined cylindrical pore with the pore radius being a function of time

The sieving coefficient is the ratio between the post-sieved and pre-sieved solute concentrations: the downstream external solute concentration (at $z = L$) divided by the upstream external solute concentration (at $z = 0$):

$$\theta_{pore} = \frac{C_L}{C_0} \tag{44}$$

As aforementioned, for a solute transport into a dead end chamber, $C_L = \langle N \rangle / \langle v \rangle$ and the sieving coefficient is

$$\theta_{pore} = \frac{C_L}{C_0} = \frac{K_c}{1 - (1 - K_c)e^{-Pe}} . \tag{45}$$

Substituting the expressions for convective hindrance factor (K_c) and the Peclet number (Pe) indicated in Eqs. (37) and (43) in Eq.(45), it can be written as

$$\theta_{pore}(t) = \frac{\left[1 - \frac{4}{3} \cdot \frac{r_s^2}{\left(R^2 + 8\mu L k_{3layer}\right)} \right]}{1 - \left\{ \left[\frac{4}{3} \cdot \frac{r_s^2}{\left(R^2 + 8\mu L k_{3layer}\right)} \right] \cdot \exp\left[-\frac{6\pi\mu r_s L \Delta \wp}{kT} \cdot \left(\frac{R^2}{8\mu L} + k_{3layer} - \frac{1}{6} \cdot \frac{R^2 r_s^2}{(\mu L)\left(R^2 + 8\mu L k_{3layer}\right)} - \frac{4}{3} \cdot \frac{r_s^2 k_{3layer}}{\left(R^2 + 8\mu L k_{3layer}\right)} \right) \right] \right\}} \tag{46}$$

Examples of calculated results for θ_{pore} as a function of the pore radius, the fluid viscosity and the pore length are given in Appendix B; the sieving coefficient remains constant (in an approximate sense) despite the changing fluid viscosity and pore length.

It is worth mentioned that the sieving coefficient (θ_{pore}) is a function of time due to the dependence of K_c and R_v on the pore radius (R) which is time dependent. The sieving coefficient averaged overall a period of a complete round of the pore opening and closing, $\langle \theta_{pore} \rangle$, is defined as

$$\left\langle \theta_{pore} \right\rangle = \frac{\frac{1}{T} \int\limits_0^T R_v(t)\,\theta(t)\, dt}{\frac{1}{T} \int\limits_0^T R_v(t)\, dt} \tag{47}$$

where, as aforementioned, R_v is volume flow rate through the cylindrical pore that can be calculated using the expression given as Eq.(20). As stated in the previous section, 2 options for R(t) are considered; that of a sine function (Eq. (18)) and a cosine function (Eq.(19)). In the present study, the average sieving coefficient is calculated by employing Eq. (47) with the integration completed by using adaptive Simpson quadrature (MATLAB, Netick, Messachusetts, USA). Calculated results are discussed in Chapter 3.

2.5.2) Calculation of the overall solute sieving coefficient across the glomerular capillary wall

The obtained $\left\langle \theta_{pore} \right\rangle$ are then utilized in the calculation of the overall sieving coefficient of solutes across the glomerular barrier, $\left\langle \theta \right\rangle$. As aforementioned, Bowman's space is viewed as a dead-end chamber with the incoming solute flux being the product of the downstream solute concentration (C_B) and the averaged fluid velocity. C_B, is therefore, can be thought as the rate at which the solutes are transported into Bowman's Space divided by the fluid volume flow rate. As discussed in Chapter 1, our calculation is completed under the assumption that the glomerular barrier consists of the three-layered filtration surface, the four-layered barrier with the mesangium located between the endothelial fenestrae and GBM, and the shear-induced opening at the junction between the filtration surface and the four-layered barrier. The total solute filtration rate is the addition of the filtration rate through the filtration surface, the mesangium and the openings. The overall sieving coefficient, the ratio between the solute concentration in Bowman's space (C_B) and the solute concentration in the capillary lumen (C_L), can be written as

$$\left\langle \theta \right\rangle = \frac{C_B}{C_L} = \frac{\left(S_{3layer}\, k_{3layer}\, \theta_{3layer}\, [\Delta\wp - \Delta\Pi] \right) + \left(S_{4layer}\, k_{4layer}\, \theta_{4layer}\, [\Delta\wp - \Delta\Pi] \right) + \left(\left\langle R_v \right\rangle \left\langle \theta_{pore} \right\rangle \right)}{SNGFR}$$

$$\tag{48}$$

Where θ_{3layer}, θ_{4layer} and θ_{pore} are sieving coefficient of the glomerular barrier with three-layered, four-layered glomerular filtration surface and pore, respectively. S_{3layer} and S_{4layer} are the glomerular filtration and glomerular mesangium surface area, respectively. k_{3layer} and k_{4layer} are the hydraulic permeability of glomerular filtration surface and glomerular mesangium, respectively. $\Delta\wp$ and $\Delta\Pi$ are hydraulic and oncotic pressure difference. Whereas R_v is volume flow rate, and SNGFR is single

nephron glomerular filtration rate. The numerator (in Eq. (48)) is the rate at which the solute is transported into the primary urine in the Bowman's space per glomerulus; the first and second term are the filtration rate through filtration surface and the glomerular mesangium, respectively, whereas the last term is the solute filtration rate through the shear flow induced openings. The denominator is the single-nephron glomerular filtration rate, the fluid filtration rate per glomerulus. The calculated overall sieving coefficients are, then, compared to the ficoll sieving coeffients obtained from in vivo urinalaysis [18,19].

Chapter 3

Results and Discussion

Calculated results are presented below, beginning with the effect of the chosen option of R(t) on the calculated average sieving coefficient of a shear-induced opening $\left(\langle\theta_{pore}\rangle\right)$ and the overall sieving coefficient across the glomerular barrier $\left(\langle\theta\rangle\right)$ in Sec.3.1 where the sieving coefficient computed by assuming that the pore radius, R(t), is a sine function is compared to sieving coefficient obtained by assuming that R(t) is a cosine function. Next, the overall sieving coefficient of a solute through the glomerular capillary wall (consisting of a glomerular filtration surface, the four-layered barrier that includes the mesangium and, as we speculate, the shear-induced pores at the junction between the two barriers) are presented as a function of number of shear-induced openings and plasma viscosity in Sec. 3.2. Finally, the comparison between the calculated overall sieving coefficient and the sieving coefficient of ficolls from urinalaysis in healthy humans [18] and patients with diabetic nephropathy [19] will be discussed in Sec.3.3.

3.1) The effects of the choices of R(t) on the averaged solute sieving coefficient through the shear-induced openings and the overall sieving coefficient through the glomerular barrier

The comparison between $\langle\theta_{pore}\rangle$ obtained under the assumption that the pore radius, R(t), is a sine function (and the shear-induced pores open and close gradually) and $\langle\theta_{pore}\rangle$ obtained from R(t) being a cosine function (under the assumption that the capillary rupture is sudden, but its closing is gradual) is given in Table 1. The presented results are calculated with the physiological parameters being those of healthy human; the GBM thickness (L) is 400 nm, and the plasma viscosity (μ) is 1.2 mPa.s. As shown in the table, $\langle\theta_{pore}\rangle$ computed by assuming that R(t) is a sine function is slightly smaller than $\langle\theta_{pore}\rangle$ calculated under the assumption that R(t) is a cosine function. This is to be expected as $\langle\theta_{pore}\rangle$ of solutes across a barrier with pores that open and close gradually should be smaller than that of solutes across a barrier with pores that open abruptly and then close down gradually over the same period of time. The comparison between $\langle\theta_{pore}\rangle$ obtained under the assumption that the pore radius, R(t), is a sine function and $\langle\theta_{pore}\rangle$ obtained from R(t) being a cosine function for a calculation using the GBM thickness and the plasma viscosity of patients with diabetic nephropathy yield the same results as shown in Table 2. ; for both cases, however, the difference is found to be less than 1%. This is due to the fact that, R_0 is much larger than r_s; for most of the range of R(t), θ_{pore} is close to 1. Therefore, $\langle\theta_{pore}\rangle$ computed by assuming that R(t) is a sine function is close to that calculated by assuming that R(t) is a cosine function.

Table 1. The comparison between $\langle \theta_{pore} \rangle$ obtained by assuming that R(t) is a sine function (Eq. (18)) and those obtained by assuming R(t) is a cosine function (Eq. (19)). The GBM thickness and plasma viscosity are those of healthy humans (L = 400 nm and μ = 1.2 mPa.s).

Solute radius (nm)	Options of R(t)		Solute radius (nm)	Options of R(t)	
	Sine	Cosine		Sine	Cosine
2.6	0.9959	0.9982	5.2	0.9903	0.9925
3.6	0.9942	0.9965	5.4	0.9897	0.9920
4.6	0.9919	0.9942	5.6	0.9891	0.9914
5.0	0.9908	0.9931			

Table 2. The comparison between $\langle \theta_{pore} \rangle$ obtained by assuming that R(t) is a sine function (Eq. (18)) and those obtained by assuming R(t) is a cosine function (Eq. (19)). The GBM thickness and plasma viscosity are those of patients with diabetic nephropathy (L = 800 nm and μ = 1.2 mPa.s).

Solute radius (nm)	Options of opening		Solute radius (nm)	Options of opening	
	Sine	Cosine		Sine	Cosine
1.6	0.9971	0.9993	5.2	0.9903	0.9926
2.0	0.9967	0.9989	5.4	0.9897	0.9920
2.6	0.9959	0.9982	5.6	0.9891	0.9914
3.6	0.9942	0.9965	5.8	0.9885	0.9907
4.6	0.9919	0.9942	6.0	0.9878	0.9901
5.0	0.9909	0.9931			

The effects of the chosen options of R(t) over the overall sieving coefficients of solutes across the glomerular capillary wall, $\langle \theta \rangle$, calculated by using Eq.(48) from the solute filtration across the three-layered filtration surface, the four-layered barrier that includes the glomerular mesangium and the shear-induced opening) are displayed in Figs. 7A (for healthy humans) and 7B (for patients with diabetic nephropathy). Also shown in the figures are sieving of ficolls from urinalaysis obtained by Blouch et al. [18] and Anderson et al. [19]. In accord with the results in Tables 1 and 2, $\langle \theta \rangle$ computed by assuming that R(t) is a sine function is graphically indistinguishable from those obtained by assuming that R(t) is a cosine function for the range of r_s from 1.6 nm to 6 nm if the opening period is assumed to be equal. For subsequent results, the employed function for R(t) is a sine function (Eq. (18)). (The difference between the calculation completed under the different options of R(t) is given in Appendix C.)
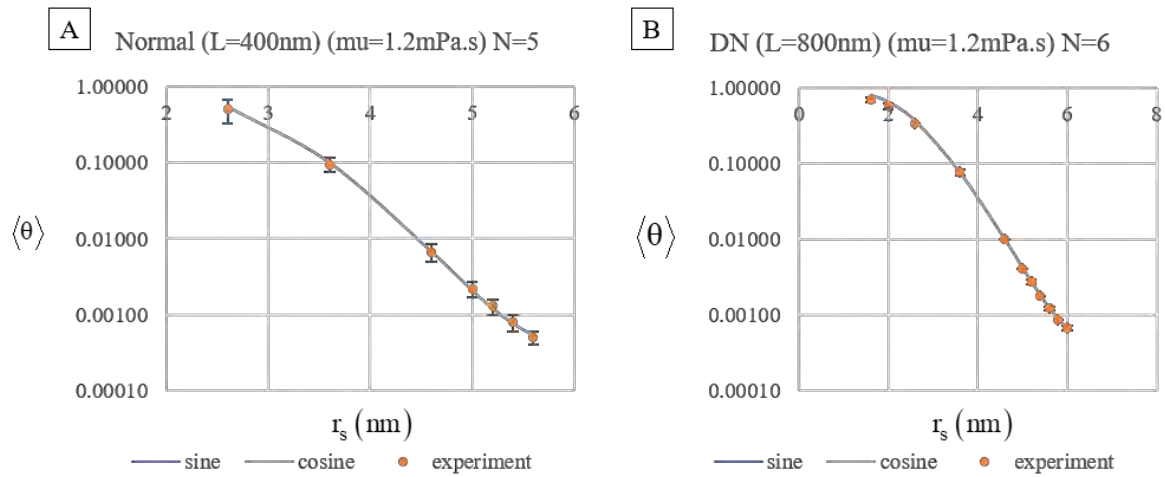
Fig. 7 The overall sieving coefficient across the glomerular barrier, $\langle\theta\rangle$ as a function of solute radius (r_s) calculated by using (A) the GBM thickness and the plasma viscosity of healthy humans and (B) the GBM thickness and the plasma viscosity of patients with diabetic nephropathy. Results completed by assuming that R(t) is a sine function (Eq. (18)) is compared to those computed by assuming that R(t) is a cosine function (Eq. (19)). Also presented are ficoll sieving coefficients from in vivo urianalysis [18,19].

3.2) Effects of the number of shear induced openings and plasma viscosity on the overall sieving coefficient across the glomerular barrier

3.2.1) The overall sieving coefficient across the glomerular capillary wall as a function of the number of shear-induced openings

The effect of the shear-induced openings on glomerular size-selectivity is demonstrated in Figs. 8A and 8B where the overall glomerular solute sieving coefficient, $\langle\theta\rangle$, of the moderate-sized solute (r_s = 2.6 nm) and that of a large solute (r_s = 5.6 nm) is presented as a function of the number of shear-induced openings per glomerulus (N). As shown in the figures, $\langle\theta\rangle$ increases as a linear function of N in accordance with the expression in Eqs. (20) and (48) where R_V and, subsequently, $\langle\theta\rangle$ are linearly dependent on N. As shown in Fig. 8A, the effect of $\langle\theta_{pore}\rangle$ and the increase in N on $\langle\theta\rangle$ of a spherical solute with r_s of 2.6 nm is quite small. The increasing N, however, has a larger effect on $\langle\theta\rangle$ of a larger solute with r_s of 5.6 nm as indicated in Fig. 8B. The same phenomena is observed for $\langle\theta\rangle$ calculated by setting the GBM thickness and other physiological parameters associated with diabetic nephropathy shown in Figs. 9A and 9B; the effect of the increase in N on $\langle\theta\rangle$ of a smaller solute with r_s of 1.6 nm is negligible, but causes a significant increase in $\langle\theta\rangle$ of a larger solute with r_s of 6.0 nm. This indicates that, although the presence of the shear-induced openings (at the junction where the filtration surface meets the glomerular mesangium) is unlikely to affect the value of the sieving coefficient of smaller solutes, it can cause a significant increase in the sieving coefficient of solutes with $r_s \geq$ 5.0 nm

Fig. 8 The total average sieving coefficient, $\langle\theta\rangle$, as a function of the number of pores, N. Results are the sieving coefficient of (A) spherical solutes with r_s = 2.6 nm and (B) that of solutes with r_s = 5.6 nm. Physiological constants and hydraulic permeabilities are those associated with healthy humans.
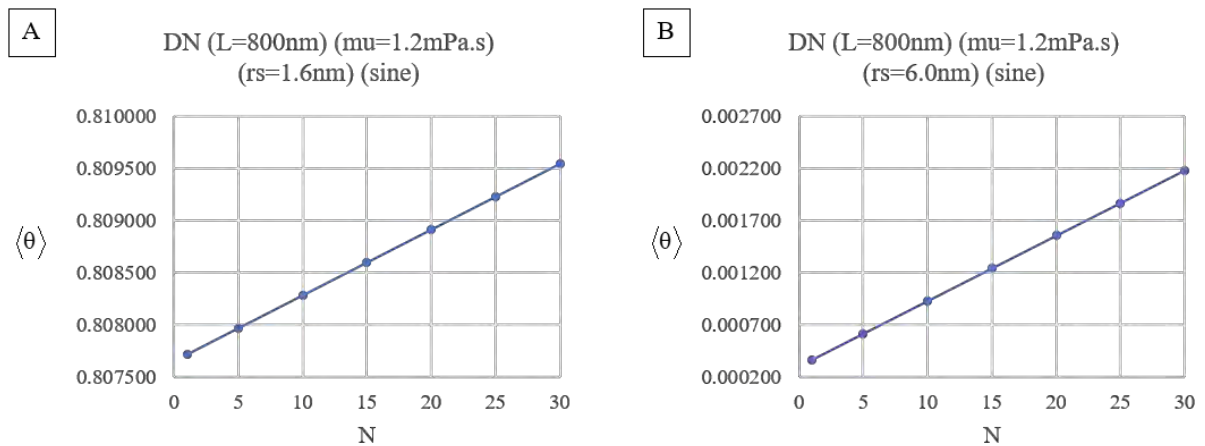
Fig. 9 The total average sieving coefficient, $\langle\theta\rangle$, as a function of the number of pores, N. Results are the sieving coefficient of (A) spherical solutes with r_s = 1.6 nm and (B) that of solutes with r_s = 6.0 nm. Physiological constants and hydraulic permeabilities are those associated with patients with diabetic nephropathy.

3.2.2) The overall sieving coefficient as a function of plasma viscosity

It is known that hyperglycemia, a high level of glucose in blood circulation, results in the increase in the viscosity of blood plasma. Experiments indicate that the plasma viscosity of patients with diabetic nephropathy are in the range of 1.2 – 1.8 mPa.s, slightly higher than the plasma viscosity of healthy humans at 1.2 mPa.s. In Figs. 10A and 10B, the effects of the plasma viscosity on the overall solute sieving coefficient across the glomerular capillary wall is examined. L = 800 nm. The increase in the plasma viscosity causes a decline in $\langle\theta\rangle$. In accordance with results presented in Sec 3.2.1 where the shear-induced openings are shown to affect $\langle\theta\rangle$ of large solutes but not those of small solutes, the

reduction of $\langle\theta\rangle$ is negligible if $r_s = 1.6$ nm as shown in Fig. 10A, but becomes larger with increasing r_s as indicated in Fig. 10B. Overall, however, the effect of the plasma viscosity is found to be small.
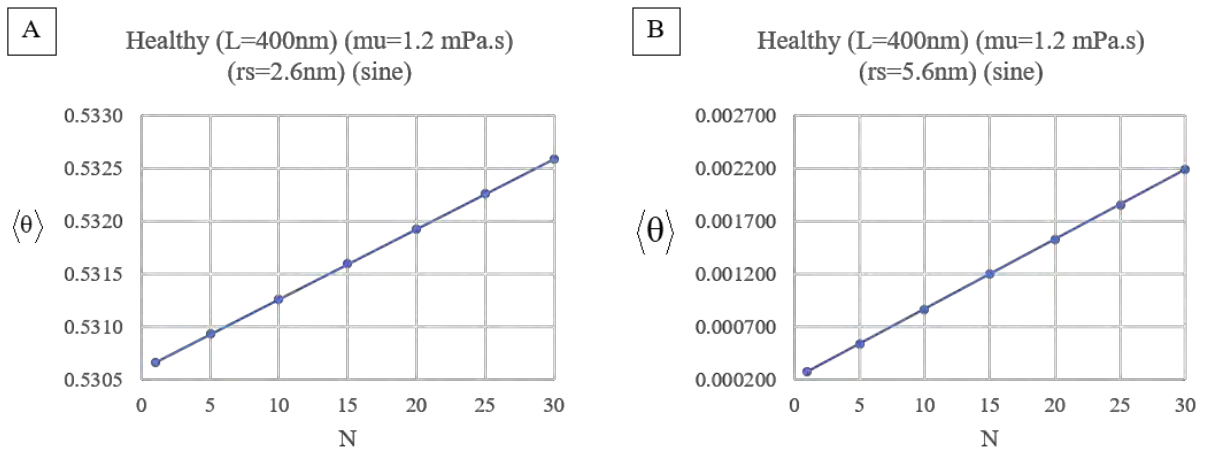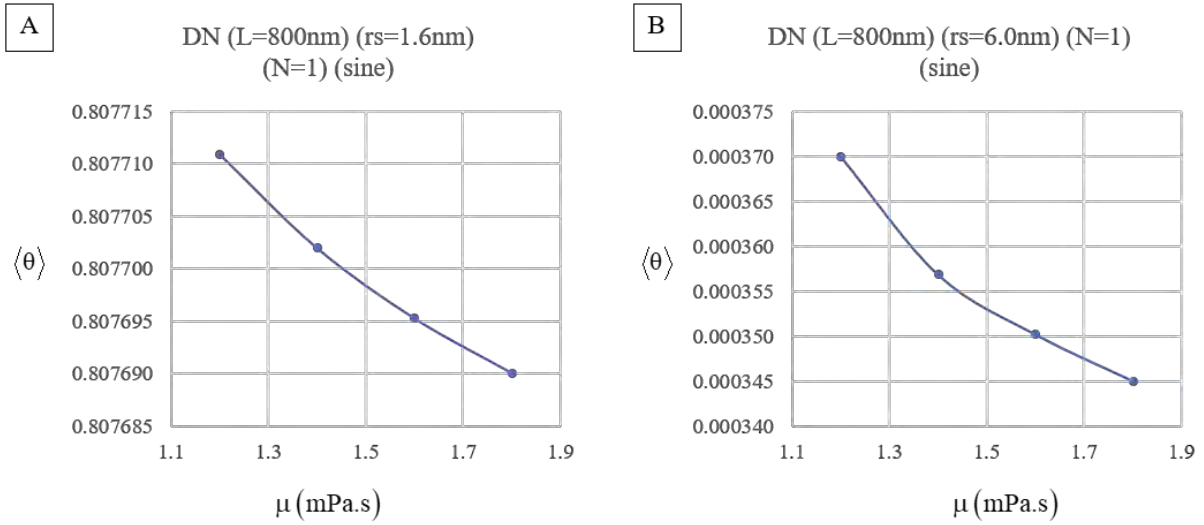

Fig. 10 The total average sieving coefficient, $\langle\theta\rangle$, as a function of the plasma viscosity, μ. Results are the sieving coefficient of (A) spherical solutes with $r_s = 1.6$ nm and (B) that of solutes with $r_s = 6.0$ nm. Physiological constants and hydraulic permeabilities are those associated with patients with diabetic nephropathy.

3.3) Comparison between the calculated sieving coefficient and the sieving coefficient of ficolls from in vivo urinalysis

3.3.1) Healthy humans

In order to examine the effect of the shear-induced openings on glomerular size-selectivity, the computed overall sieving coefficient across the glomerular barrier $(\langle\theta\rangle)$ is compared to the sieving coefficient of ficolls from urianalysis performed in humans [18, 19]. In Fig. 11, $\langle\theta\rangle$ computed by employing physiological parameters and, subsequently, the hydraulic permeability typically found in healthy humans, is presented as a function of r_s and compared to ficoll sieving coefficient obtained from urinanalysis performed in healthy humans [18] presented as filled symbols. Also presented in the figure is $\langle\theta\rangle$ calculated without including the effect of the solute filtration through the shear-induced opening (plotted as a grey dashed line). As aforementioned, $\langle\theta\rangle$ computed with N = 0 agrees well with the experimental results if $r_s \le 4.5$ nm, but significantly overestimates the sieving coefficient if $r_s > 5.0$ nm. In accord with results in Sec. 3.2 and 3.3, the presence of the openings does not significantly affect $\langle\theta\rangle$ of small and medium-sized solutes (with $r_s \le 4.5$ nm) but increases $\langle\theta\rangle$ of larger solutes. As N increases, $\langle\theta\rangle$ increases and becomes graphically distinguishable from $\langle\theta\rangle$ calculated by assuming that N = 0. As

shown in Fig. 11, the value of N that yield $\langle\theta\rangle$ with the least deviation from the ficoll sieving coefficient is N = 5.
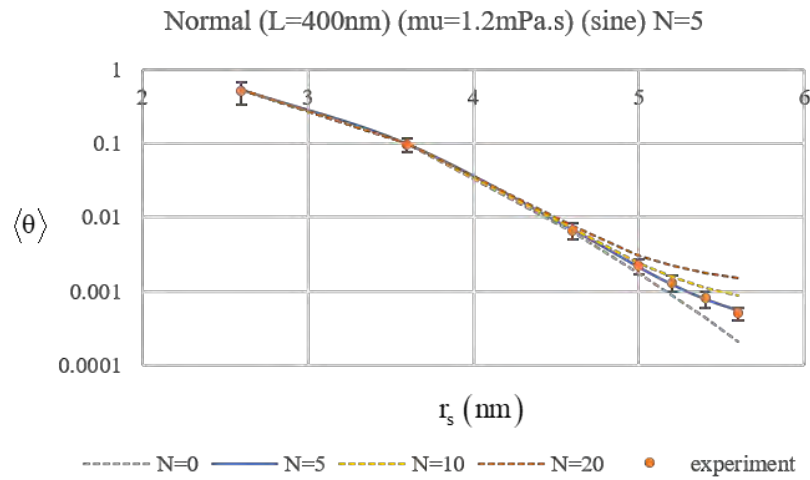
Normal (L=400nm) (mu=1.2mPa.s) (sine) N=5

Fig. 11 The computed overall sieving coefficient across the glomerular barrier $\left(\langle\langle\theta\rangle\rangle\right)$ computed using the physiological parameters typically found in healthy humans as a function of solute radii. Results are presented for N = 0 (a grey dashed line), N = 10 (a yellow dashed line), N = 20 (a red dashed line) and N = 5 (a solid line). Also presented is the ficoll sieving coefficient obtained from in vivo urianalysis in healthy humans [18].

3.3.2) Patients with diabetic nephropathy

Next, the effect of the shear-induced openings on glomerular size-selectivity in the case of patients with diabetic nephropathy is investigated. As shown in Fig. 12, the overall sieving coefficients $\left(\langle\theta\rangle\right)$ computed by assuming that N = 0, 6, 20, and 30 and utilizing the physiological parameters associated with diabetic nephropathy are presented as a function of solute radii (r_s). Also presented in the figure is the sieving coefficient of ficolls from in vivo urinalysis with the test subjects being patients with early-but-overt diabetic nephropathy [19] shown as filled symbols. μ = 1.2 mPa.s (equal to that of healthy humans). The observed trend is similar to that of results (computed using the physiological parameters found in healthy humans) presented in Fig. 11. $\langle\theta\rangle$ computed by assuming that N = 0 (which indicates that shear-induced openings are absent) agrees well with the ficoll sieving coefficient with $r_s \leq$ 4.5 nm but overestimates the value of $\langle\theta\rangle$ if the solute radius is larger. If the shear-induced openings are present (N > 0), the sieving coefficients of solutes with $r_s \leq$ 4.5 nm hardly change, whereas $\langle\theta\rangle$ of solutes with $r_s >$ 4.5 nm significantly increases and becomes graphically distinguishable from $\langle\theta\rangle$ computed with N = 0. As shown in the figure, the value of N that yields $\langle\theta\rangle$ that is closest to the ficoll sieving coefficient from the experiment is N = 6, slightly larger but very close to the value of N that yields $\langle\theta\rangle$ with the smallest deviation from the experimental results in the case of healthy humans (N = 5). As shown in Figs. 13 and 14, if the employed value of the plasma viscosity increases, the value of N that yields $\langle\theta\rangle$

with the smallest difference from the sieving coefficient of ficolls [19] increases. For instance, if $\mu = 1.8$ mPa.s, the value of N that yields $\langle \theta \rangle$ with the smallest deviation from the experimental results is N = 9.

It can be concluded that the value of N that $\langle \theta \rangle$ that agrees well with the experimentally obtained sieving coefficient in the case of patients with diabetic nephropathy is slightly higher than that of healthy humans. This might be due to the fact that, with diabetic nephropathy associated with the surface area of the filtration surface, the higher averaged fluid velocity through the filtration surface, and the denser glomerular mesangium, the non-uniformity of the flow velocity at the junction where the filtration surface meets the glomerular mesangium is likely to be greater than that in healthy humans. With the gradient of the flow velocity of the shear flow at the junction being larger, the possibility of the occurrence of shear-induced openings is likely to be higher if diabetic nephropathy is present. Nevertheless, in the cases of healthy humans and patients with diabetic nephropathy, the value of N that yields $\langle \theta \rangle$ that agrees well with the experimentally obtained sieving coefficient is low enough such that, given that the openings periodically opens and closes, hematuria is unlikely to occur. This agrees with the medical finding that, even though hematuria is sometimes found in patients with diabetic nephropathy, it is not a common symptom.
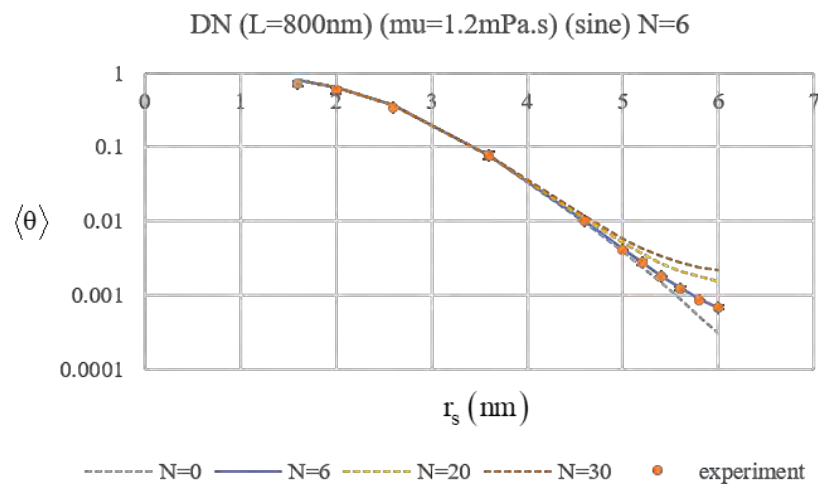
Fig. 12 The computed overall sieving coefficient across the glomerular barrier $\left(\langle \theta \rangle \right)$ computed using the physiological parameters typically found in patients with diabetic nephropathy as a function of solute radii. Results are presented for N = 0 (a grey dashed line), N = 20 (a yellow dashed line), N = 30 (a red dashed line) and N = 6 (a solid line). $\mu = 1.2$ mPa.s. Also presented is the ficoll sieving coefficient obtained from in vivo urianalysis in patients with diabetic nephropathy [19].
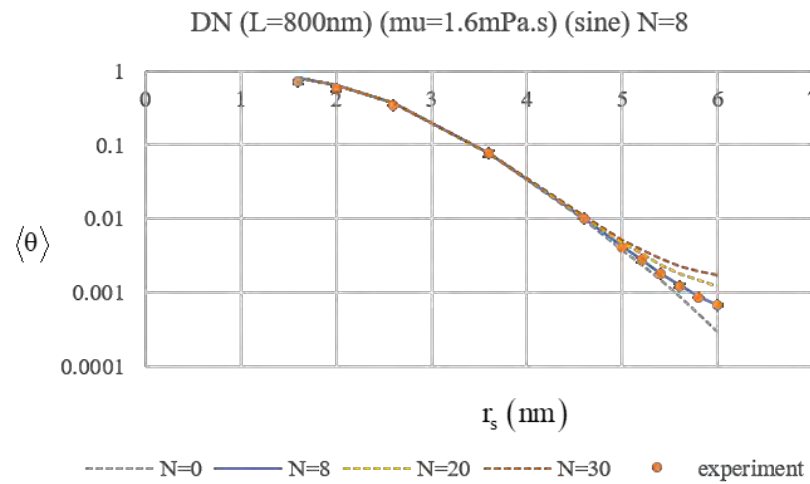
Fig. 13 The computed overall sieving coefficient across the glomerular barrier $\left(\langle\theta\rangle\right)$ computed using the physiological parameters typically found in patients with diabetic nephropathy as a function of solute radii. Results are presented for N = 0 (a grey dashed line), N = 20 (a yellow dashed line), N = 30 (a red dashed line) and N = 8 (a solid line). μ = 1.6 mPa.s. Also presented is the ficoll sieving coefficient obtained from in vivo urianalysis in patients with diabetic nephropathy [19].
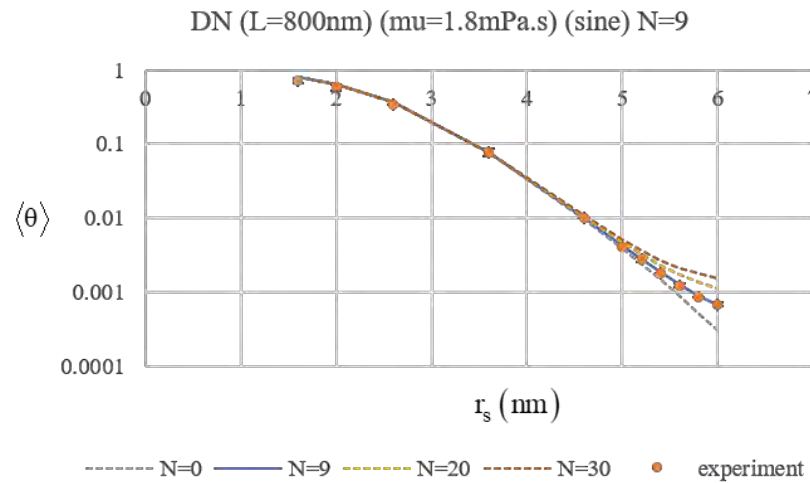
Fig. 14 The computed overall sieving coefficient across the glomerular barrier $\left(\langle\theta\rangle\right)$ computed using the physiological parameters typically found in patients with diabetic nephropathy as a function of solute radii. Results are presented for N = 0 (a grey dashed line), N = 20 (a yellow dashed line), N = 30 (a red dashed line) and N = 9 (a solid line). μ = 1.8 mPa.s. Also presented is the ficoll sieving coefficient obtained from in vivo urianalysis in patients with diabetic nephropathy [19].

Chapter 4

Conclusion

Glomerular selectivity remains an enigma despite several decades of on-going research. A refine biological filtration device, the glomerular capillary wall is believed to consist of the three-layered filtration surface (that accounts for two-third of its entire surface) and the four-layered barrier that includes the glomerular mesangium (with the surface area being one-third of the total glomerular capillary surface). Previous calculations performed by assuming that the solutes are transported through the glomerular filtration surface and the four-layered barrier, although yields the solute sieving coefficient that agrees well with the ficoll sieving coefficient obtained from *in vivo* urinalysis if the solute radius is less than or equal to 4.5 nm, significantly underestimate the solute coefficient if the solute is larger. A small amount of red blood cells found in urine of healthy humans and patients with diabetic nephropathy, as well as electron micrographs (performed with the test subjects displaying a symptom of thin GBM) demonstrating red blood cells escaping through the openings at the junction between the glomerular filtration surface and the glomerular mesangium where the shear flow is found leads to a speculation that shear flow induced openings at the junction may occur and may serve as another pathway for glomerular solute filtration. In the present study, the possible contribution of these shear flow induced openings on glomerular size-selectivity is theoretically investigated using low-Reynolds-number hydrodynamics and hindered transport theory with the openings assumed to be pores that periodically open and close. Calculated results indicate that solute filtration through these pores does not significantly alter the sieving coefficient of small and medium-sized solutes but considerably increases the sieving coefficient of solutes with the radius greater than 4.5 nm. If a small number of the pores are present, the computed sieving coefficients agree with those of ficoll obtained from urinalysis performed in healthy humans and patients with diabetic nephropathy for the entire range of solute size with the values of SNGFR also agrees with those reported in the same experiments. It is worth noting, however, that the micrographs showing the red blood cell escapes through the glomerular capillary wall opening were obtained from glomeruli of patients with abnormal GBM and a symptom of hematuria. The same experimental evidence for cases of healthy humans and patients with diabetic nephropathy are yet to be found.

References

[1] J. Gordon Betts, William Blaker et al. Aug 20, 2019. Chapter 25, The Urinary System. "Anatomy and Physiology". Rice University, pp.1209.

[2] Matterm, K. J., 2008, "Permeability Studies in Biomimetic Glycosaminoglycan Hydrogel Membranes", Ph.D. thesis, Massachusetts Institute of Technology, Cambridge' MA.

[3] Heraldsson, B., Nystrom, J., & Deen, W. M. 2008. "Properties of the Glomerular Barrier and Mechanisms of Proteinuria." Physiological Reviews, 88(2), 451-487. Doi:10.01152/physrev.00055.2006

[4] Science Direct, 2019. "Mesangial Cell," Retrieved from https://www.sciencedirect.com/topics/agricultural-and-biological-sciences/mesangial-cell

[5] Genjiro Kimura, Masahito Imanishi et al, 2019, "Intrarenal Hemodynamics in Patients with Essential Hypertension," AHA/ASA Journals, pp. 421-428.

[6] C. R. Neal and C. C. Michael. 1996, "Opening in frog microvascular endothelium by high intracellular pressures," Journal of Physiology, 492.1, pp. 39-52.

[7] National Institute of Diabetes and Digestive and Kidney Disease. "Hematuria (Blood in the Urine)," Retrieved from https://www.niddk.nih.gov/health-information/urologic-diseases/hematuria-blood-urine

[8] Jill E. Collar, Suresh Ladva, Thomas D.H. Cairams, and Victoria Cattell. 2001, "Red ccell traverse through thin glomerular basement membranes." Kidney International, Vol. 59, pp. 2069-2072.

[9] William M. Deen. 1998, "Analysis of Transport Phenomena: Scaling and approximation technique," New York: Oxford university press.

[10] Panadda Dechadilok. "เอกสารประกอบการสอนวิชา 2304520,".

[11] W. M. Deen. 1987, "Hindered Transport of Large Molecule in Liquid-Filled Pores," AIChE Journal, Vol.33, No.9, pp. 1409-1425.

[12] Panadda Dechadilok and William M. Deen. 2006, "Hindrance Factors for Diffusion and Convection in Pores," Ind. Eng. Chem. Res. 2006, 45, 6953-6959.

[13] Donale E. McMillan. 1974, "Disturbance of Serum Viscosity in Diabetes Mellitus," Diabetes Research Division, Sansum Medical Research Foundation, Santa Barbara, California 93105. The Journal of Clinical Investigation Volume 53 April 1974 1071-1079.

[14] Brun JF, Aloulou I, Varlet-Marie E. 2004, "Type 2 Diabetics with Higher Plasma Viscosity Exhibit a Higher Blood Pressure," US National Library of Medicine National Institute of Health.

[15] W. H. S. George. "Relative Plasma Viscosity with Reference to Patients with Diabetes Mellitus," Department of chemical pathology, the city hospital, Derby.

[16] G Caimi, D Sinagra, AM Scarpitta and R Lo Presti. 2001, "Plasma Viscosity and Insulin Resistance in Metabolic Syndrome," International Journal of Obesity 25, 1856 – 1857.

[17] OP Kulshrestha, Madhu Mathur. 1983, "Plasma Viscosity in Diabetic Retinopathy," Indian journal ophthalmology, volume 31, issue 5, page 543-544.

[18] Kristins Blouch, Willium M. Deen, Lean-Pierre Fauvel, Joan Blalek, eraldine Derby, and Bryan D. Myers. 1997, "Molecular Configuration and Glomerular Size Selectivity in Health and Nephrotic Humans," the American Physiological Society, 0363-6127/97, F430-F437.

[19] Steen Anderson, Kristina Blouch, Joan Bialek, Marja Deckert, Hans-Henrik Parving, and Bryan D. Myers. 2000, "Glomerular Permselectivity in Early Stages of Overt Diabetic Nephropathy," International Society of Nephrology, Kidney International, Vol. 58, pp. 2129-2137.

[20] William El. DEEN. 1998, :Analysis of transport phenomena". Oxford University Press

Appendix A

A-1) The effect of volume flow rate of pore per glomerulus on the hydrodynamic pressure difference and single nephron glomerular filtration rate

Calculation of effect of volume flow rate $\left(\langle R_v \rangle_{pore}\right)$ on the hydrodynamic pressure difference $(\Delta\wp)$ and single nephron glomerular filtration rate (SNGFR) are presented below in Fig. A-1. If the hydraulic pressure difference is constant, the effect of $\langle R_v \rangle_{pore}$ on SNGFR is as shown below.

$$SNGFR = k_{3layer}S_{3layer}\left(\Delta\wp - \Delta\Pi\right) + k_{4layer}S_{4layer}\left(\Delta\wp - \Delta\Pi\right) + \langle R_v \rangle_{pore} \tag{A-1}$$

where k_{3layer} and k_{4layer} are hydraulic permeability of glomerular filtration surface and glomerular mesangium, respectively. S_{3layer} and S_{4layer} are glomerular filtration and glomerular mesangium surface area. $\Delta\Pi$ is an oncotic pressure difference.

If on the other hand, SNGFR is assumed to be constant, the effect of volume flow rate through the opening on hydraulic pressure difference can be calculated as

$$\Delta\wp = \frac{SNGFR + S_{3layer}k_{3layer}\Delta\Pi + S_{4layer}k_{4layer}\Delta\Pi}{S_{3layer}k_{3layer} + S_{4layer}k_{4layer} + N\pi\left[\dfrac{3}{6}\dfrac{R_0^4}{\mu L} + \dfrac{1}{2}k_{3layer}R_0^2\right]} \; . \tag{A-2}$$

For healthy humans, the effect of an inclusion of $\langle R_v \rangle_{pore}$ decreases the hydraulic pressure difference but increases SNGFR as show in Figs. A-1(A) and A-1(B).
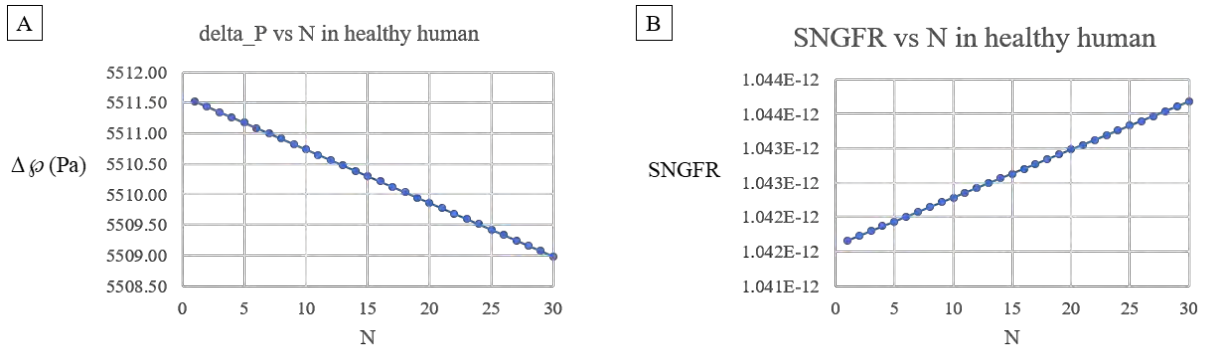
Fig. A-1 The effect of volume flow rate on hydraulic pressure difference $(\Delta\wp)$ and single nephron glomerular filtration rate (SNGFR) in normal human, as graph (A) and (B), respectively. The pressure difference decline when the volume flow rate through the pore increase (the number of pore increase) but decreasing of hydraulic pressure difference is less than 1% compared to absence of pore. Whereas SNGFR increase with volume flow rate through the pore where increasing less than 1%.

As shown in Fig. A-1, the effect of the incorporation of $\langle R_v \rangle_{pore}$ on both SNGFR (if the hydraulic pressure is assumed to be constant) and $\Delta \wp$ (when SNGFR is kept constant) creates very little alterations.

In the case of patients with diabetic nephropathies, the effect of an inclusion of $\langle R_v \rangle_{pore}$ on SNGFR (if the hydraulic pressure is assumed to be constant) and $\Delta \wp$ (when SNGFR is kept constant) are shown below in Figs. A-2(A) and A-2(B).
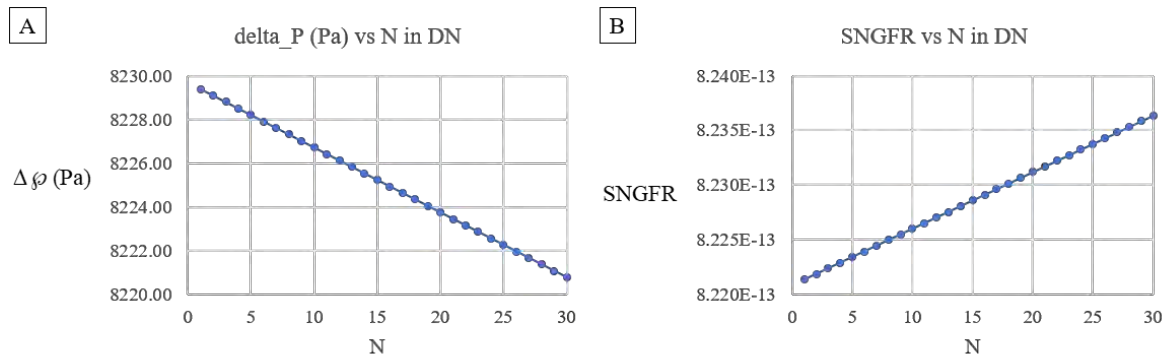
Fig. A-2 The effect of volume flow rate through the pore on hydraulic pressure difference $\left(\Delta \wp \right)$ and SNGFR in diabetic nephropathies. In graph (A), the pressure difference decreases when the volume flow rate through the pore increase but decreasing of hydraulic pressure difference is less than 1% compared to absence of pore. Whereas in graph (B), SNGFR increase with volume flow rate through the pore where increasing less than 1%.

According to the figures, the hydraulic pressure difference will decrease when with the number of pores increase, whereas SNGFR increases as a function of N. The effect of including $\langle R_v \rangle_{pore}$, however, is less than 1% (compared to results calculated with N = 0). Therefore, the hydraulic pressure difference and SNGFR are same as the previously employed in the calculation in absence of opening pore.

Appendix B

B-1) The sieving coefficient of pore

The sieving coefficient and average sieving coefficient of pore are calculated by Eqs.(47) and (48) as show in Sec.2.5. First, calculated results in Sec B-1.1 to B-1.3 are the sieving coefficient of pore as a function of pore radius, glomerular basement membrane (GBM thickness) and plasma viscosity, respectively. Second, the average sieving coefficients averaged over the period of pore opening is shown as a function of GBM thickness, plasma viscosity and solute radius.

B-1.1) The sieving coefficient of pore as a function of pore radius

The relation between the pore sieving coefficient and pore radius is shown in Fig. B-1. Graph (A) and (B) demonstrate that relation between θ_{pore} as a function of R(t).
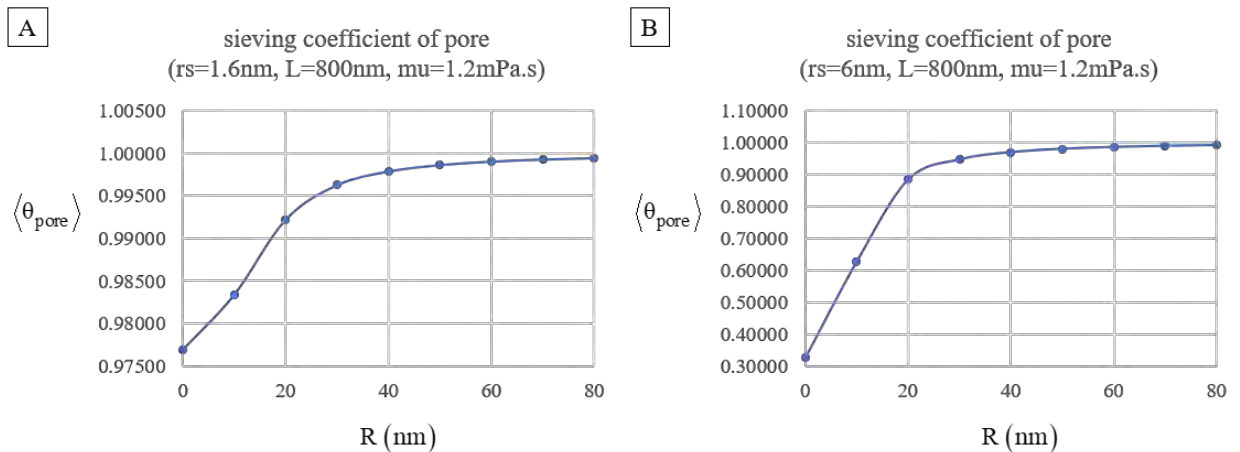
Fig. B-1 The solute coefficients of pore as a function of pore radius when plasma viscosity is 1.2 mPa.s and 800 nm of glomerular barrier thickness. (A) solute radius is 1.6 nm, the sieving coefficient of pore slight increase with rising pore radius. (B) solute radius is 6.0 nm, the sieving coefficient increased sharply with increasing pore radius.

B-1.2) The sieving coefficient as a function of GBM thickness

The sieving coefficients of pore as a function of GBM thickness are shown in Fig. B-2. Graph (A) and (B) show that relation when plasma viscosity and pore radius are fixed to 1.2 mPa.s and 80 nm, respectively. whereas the solute radius in graph A and B are 1.6 and 6.0 nm, respectively.

A

sieving coefficient of pore
(rs=1.6nm, R=R0=80nm, mu=1.2mPa.s)

$\langle \theta_{pore} \rangle$

B

sieving coefficient of pore
(rs=6.0nm, R=R0=80nm, mu=1.2mPa.s)

$\langle \theta_{pore} \rangle$
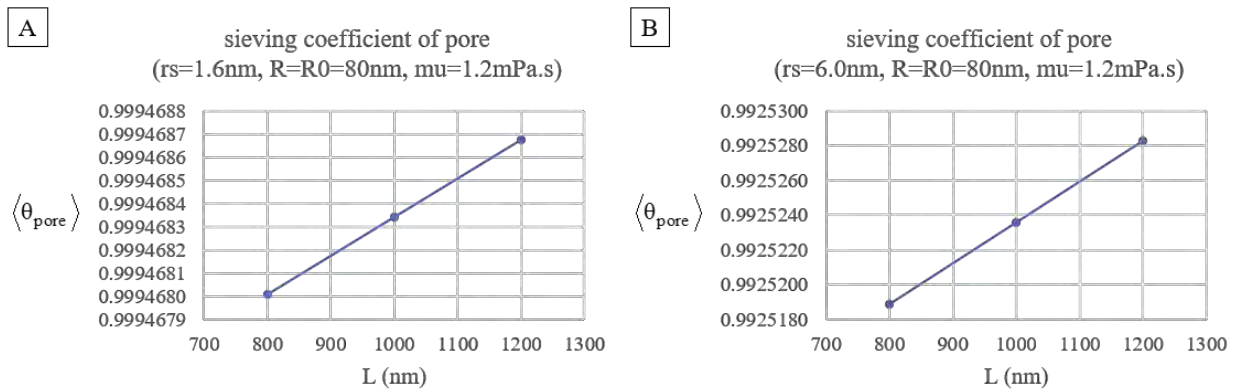
Fig. B-2 The solute coefficient of pore as a function of GBM thickness when plasma viscosity is 1.2 mPa.s and pore radius is 80 nm. (A) solute radius is 1.6 nm, the sieving coefficient of pore slight increase with rising thickness. (B) solute radius is 6.0 nm, the sieving coefficient increased sharply with thickness rise.

According to the Figs. B-2A and B-2B, the sieving coefficient of pore increase with increasing GBM thickness. In graph A, the sieving coefficient of pore that GBM thickness is 1200 nm increase about 7×10^{-5} % from the case of 800 nm. On the contrary, the sieving coefficient of pore where solute radius 6.0 nm (graph B), the sieving coefficient that thickness 1200 nm rises about 9×10^{-4} % from the sieving coefficient that GBM thickness 800 nm. Although, the increasing of the sieving coefficient of pore is very slightly, but the increasing ratio of the sieving coefficient that solute radius 6.0 nm more than about 10 times solute radius 1.6 nm.; consequently, the sieving coefficient of pore for large solute gave higher increasing ratio than small solute. However, the rising of the sieving coefficients of pore as GBM thickness are negligible, that seem to be constant.

B-1.3) The sieving coefficient as a function of plasma viscosity

The sieving coefficient of pore as a function of plasma viscosity is shown in Fig. B-3A and B-3B. The GBM thickness and pore radius are fixed to 800 and 80 nm, respectively, whereas the solute radius in graph (A) and (B) are 1.6 and 6.0 nm, respectively.

A

sieving coefficient of pore
(rs=1.6nm, R=R0=80nm, L=800nm)

$\langle \theta_{pore} \rangle$

B

sieving coefficient of pore
(rs=6.0nm, R=R0=80nm, L=800nm)
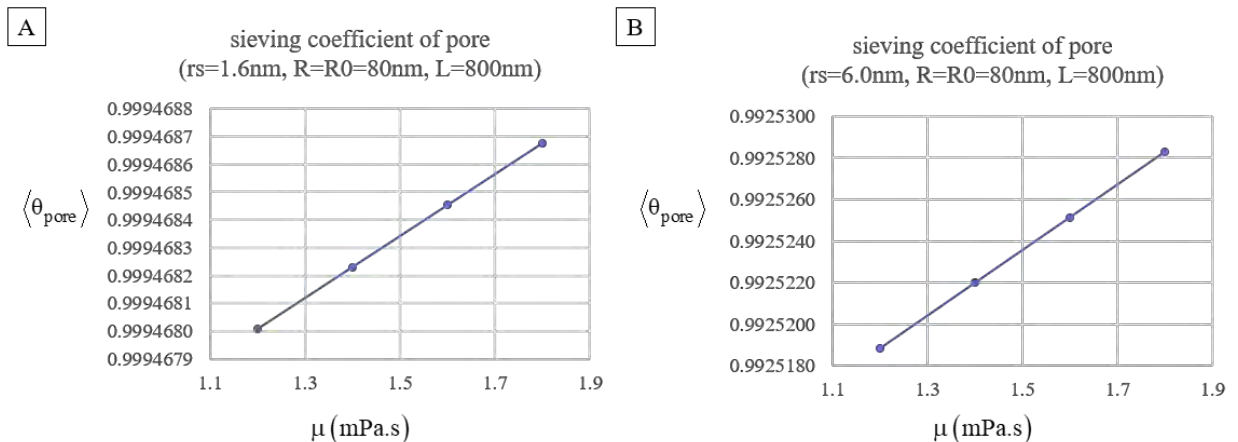
$\langle \theta_{pore} \rangle$

Fig. B-3 The solute coefficient of pore as a function of plasma viscosity when GBM thickness and pore radius are fixed to 800 and 80 nm, respectively. (A) solute radius is 1.6 nm, the sieving coefficient of pore slight increase with rising plasma viscosity. (B) solute radius is 6.0 nm, the sieving coefficient increased slightly with increasing viscosity.

According to the Fig. B-3A and B-3B, the average sieving coefficient of solute through the pore as a function of plasma viscosity. (The increases is about about 7 x 10^{-5} % from the case that plasma viscosity is 1.2 mPa.s. In contrast to the sieving coefficient of pore where solute radius 6.0 nm (graph (B)), the sieving coefficient of pore for plasma viscosity 1.8 mPa.s rises approximately 9 x 10^{-4} % compared with case plasma viscosity 1.2 mPa.s. Though, the sieving coefficient of pore very slight increase, but the increasing ratio of the sieving coefficient of pore that solute radius 6.0 nm more than about 10 times for solute radius 1.6 nm; consequently, the sieving coefficient of pore for large solute gave higher increasing ratio than small solute. Nevertheless, the sieving coefficient of pore increased very slightly, that seem to be constant.

B-2) The total average sieving coefficient as a function of GBM thickness

The total average sieving coefficient is plotted as a function of GBM thickness where opening pore as a sine function, plasma viscosity 1.2 mPa.s, single pore and solute radiuses are 1.6, 5.2, 5.4 and 6.0 nm, as show in graph (A), (B), (C) and (D) Fig. B-4., respectively.
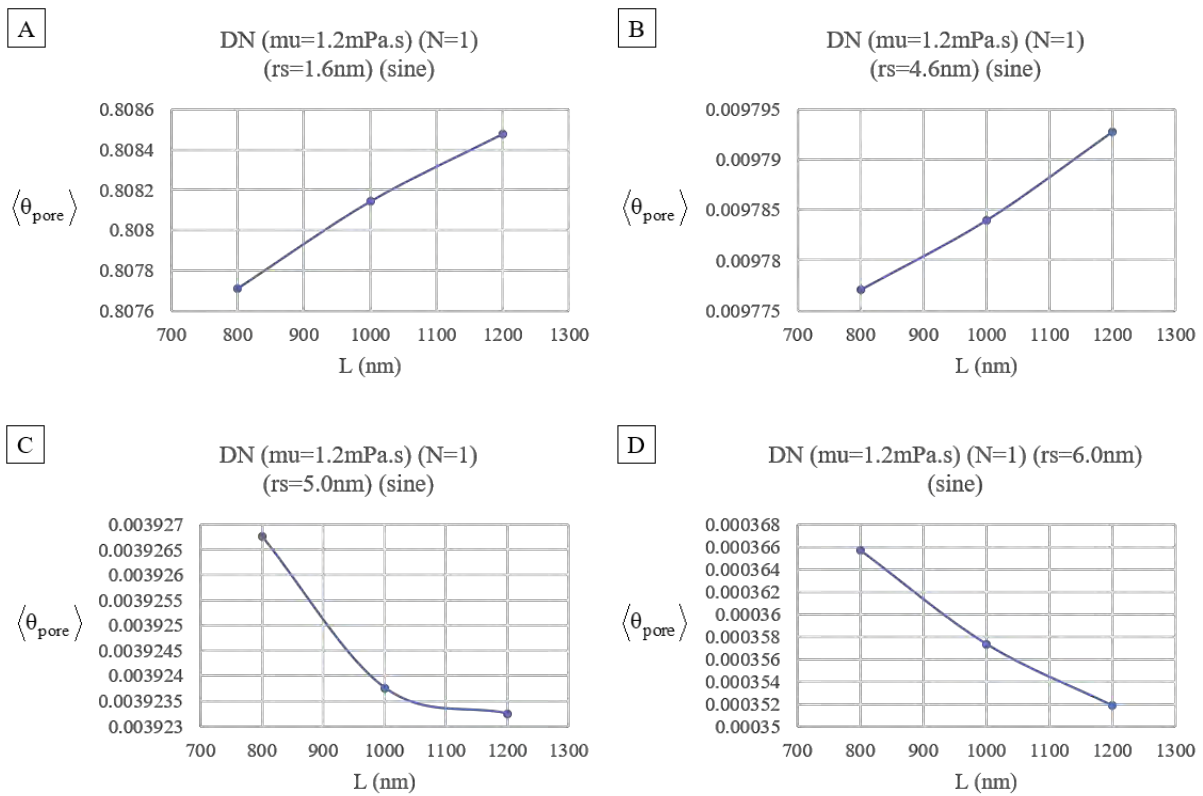
Fig. B-4 The total average sieving coefficient as a function of GBM thickness. Graph (A) to (D) show the total average sieving coefficient is plotted as a function of GBM thickness with plasma viscosity 1.2 mPa.s, single pore and solute radius 1.6, 5.2, 5.4 and 6.0 respectively. In graph (A) and (B), the total sieving coefficient rise as GMB thickness. In graph (C), the total average sieving coefficient increase in range of GBM thickness from 800 to 1000 nm, while decrease as GBM thickness from 1000 to 1200 nm. Whereas in graph (D), the total average sieving coefficient decline when GBM thickness rise.

According to Fig. B-4., graph (A) has solute radius 1.6 nm, show the total average sieving coefficient rises as GBM thickness, where increasing ratio of thickness 1200 nm compared with 800 nm

is about 0.14%. Graph (B) has solute radius 5.2 nm, the total average sieving coefficient increase considerably when GBM thickness in range of 800 to 1000 nm but increase slightly when range of GBM thickness from 1000 to 1200 nm. Graph (C) has solute radius 5.6 nm, increase when GBM thickness in range of 800 to 1000 nm but decrease when GBM thickness in range of 1000 to 1200 nm. In contrast, the total average sieving coefficient decrease with GBM is thicker when solute radius 6.0 nm as show in graph (D), where decreasing ratio between thickness 1200 and 800 nm is about 1.36%. These show the total average sieving coefficient increase as a function of GBM thickness for small solute but decrease for large solute, where the increasing and decreasing ratio depend on solute size.

Appendix C

Table C-1. The average sieving coefficient of pore with varies solute radius in healthy human, where the opening is function of sine and cosine in range of solute radius 2.6 to 5.6 nm

	Options of opening			Options of opening	
Solute radius (nm)	Sine	Cosine	Solute radius (nm)	Sine	Cosine
2.6	0.9959	0.9982	4.2	0.9929	0.9952
2.8	0.9956	0.9979	4.4	0.9924	0.9947
3.0	0.9953	0.9975	4.6	0.9919	0.9942
3.2	0.9949	0.9972	4.8	0.9914	0.9937
3.4	0.9946	0.9968	5.0	0.9908	0.9931
3.6	0.9942	0.9965	5.2	0.9903	0.9925
3.8	0.9938	0.9960	5.4	0.9897	0.9920
4.0	0.9933	0.9956	5.6	0.9891	0.9914

Table C-2. The average sieving coefficient of pore with varies solute radius in diabetic nephropathy patients, where the opening is function of sine and cosine in range of solute radius 1.6 to 6.0 nm, GBM thickness 800 – 1200 nm and plasma viscosity 1.2 - 1.8 mPa.s.

	Options of opening			Options of opening	
Solute radius (nm)	Sine	Cosine	Solute radius (nm)	Sine	Cosine
1.6	0.9971	0.9993	4.0	0.9933 – 0.9934	0.9956
1.8	0.9969	0.9991	4.2	0.9929	0.9952
2.0	0.9967	0.9989	4.4	0.9924	0.9947
2.2	0.9964	0.9987	4.6	0.9919	0.9942
2.4	0.9962	0.9984	4.8	0.9914	0.9937
2.6	0.9959	0.9982	5.0	0.9908 – 0.9909	0.9931
2.8	0.9956	0.9979	5.2	0.9903	0.9926
3.0	0.9953	0.9975 – 0.9976	5.4	0.9897	0.9920
3.2	0.9949 - 0.9950	0.9972	5.6	0.9891	0.9914
3.4	0.9946	0.9968	5.8	0.9885	0.9907
3.6	0.9942	0.9965	6.0	0.9878	0.9901
3.8	0.9938	0.9960 - 0.9961			

Table C-3 The calculated overall average sieving coefficient in diabetic nephropathies with 6 pore that opening as a function of sine and cosine, plasma viscosity 1.2 mPa.s and GBM thickness 800 nm.

Solute radius (nm)	Options of opening		Solute radius (nm)	Options of opening	
	Sine	Cosine		Sine	Cosine
1.6	0.80803	0.80803	4.0	0.03526	0.03526
1.8	0.73480	0.73480	4.2	0.02349	0.02349
2.0	0.64851	0.64851	4.4	0.01546	0.01547
2.2	0.55381	0.55381	4.6	0.01009	0.01009
2.4	0.45688	0.45689	4.8	0.00654	0.00655
2.6	0.36416	0.36416	5.0	0.00424	0.00424
2.8	0.28090	0.28090	5.2	0.00276	0.00276
3.0	0.21028	0.21028	5.4	0.00183	0.00183
3.2	0.15327	0.15327	5.6	0.00125	0.00125
3.4	0.10914	0.10914	5.8	0.00089	0.00089
3.6	0.07616	0.07616	6.0	0.00068	0.00068
3.8	0.05222	0.05222			

Table C-4 The calculated overall average sieving coefficient in diabetic nephropathies with 8 pore that opening as a function of sine and cosine, plasma viscosity 1.6 mPa.s and GBM thickness 800 nm.

Solute radius (nm)	Options of opening		Solute radius (nm)	Options of opening	
	Sine	Cosine		Sine	Cosine
1.6	0.80803	0.80803	4.0	0.03526	0.03526
1.8	0.73480	0.73480	4.2	0.02349	0.02349
2.0	0.64851	0.64851	4.4	0.01547	0.01547
2.2	0.55381	0.55381	4.6	0.01009	0.01009
2.4	0.45688	0.45689	4.8	0.00654	0.00655
2.6	0.36416	0.36416	5.0	0.00424	0.00424
2.8	0.28090	0.28090	5.2	0.00276	0.00276
3.0	0.21028	0.21028	5.4	0.00183	0.00183
3.2	0.15327	0.15327	5.6	0.00125	0.00125
3.4	0.10914	0.10914	5.8	0.00089	0.00089
3.6	0.07616	0.07616	6.0	0.00068	0.00068
3.8	0.05222	0.05222			

Table C-5 The calculated overall average sieving coefficient in diabetic nephropathies with 9 pore that opening as a function of sine and cosine, plasma viscosity 1.8 mPa.s and GBM thickness 800 nm.

Solute radius (nm)	Options of opening		Solute radius (nm)	Options of opening	
	Sine	Cosine		Sine	Cosine
1.6	0.80803	0.80803	4.0	0.03526	0.03526
1.8	0.73480	0.73480	4.2	0.02349	0.02349
2.0	0.64851	0.64851	4.4	0.01547	0.01547
2.2	0.55381	0.55381	4.6	0.01009	0.01009
2.4	0.45689	0.45689	4.8	0.00654	0.00655
2.6	0.36416	0.36416	5.0	0.00424	0.00424
2.8	0.28090	0.28090	5.2	0.00276	0.00276
3.0	0.21028	0.21028	5.4	0.00183	0.00183
3.2	0.15327	0.15327	5.6	0.00125	0.00125
3.4	0.10914	0.10914	5.8	0.00089	0.00089
3.6	0.07616	0.07617	6.0	0.00068	0.00068
3.8	0.05222	0.05222			

Appendix D

The average volume flow rate of pore that R(t) is a sine and cosine function

Volume flow rate average over the pore cross-section, as shown below

$$\langle R_v \rangle_{pore} = \frac{N\pi\Delta\wp}{\tau} \int_0^\tau \left(\frac{R^4}{8\mu L} + k_{3layer} R^2 \right) dt \tag{D-1}$$

$$\langle R_v \rangle_{pore} = \frac{N\pi\Delta\wp}{\tau} \left[\int_0^\tau \frac{R^4}{8\mu L} dt + \int_0^\tau k_{3layer} R^2 dt \right] \tag{D-2}$$

We consider two possible choices for the pore radius as a function of sine and cosine. In case of R(t) is a sine function, as shown below.

$$R = R_0 \sin\left(\frac{\pi t}{\tau} \right) \tag{D-3}$$

substitutions of expression in Eq.(D-3) into Eq.(D-2) yield the following for the averaged volume flow rate.

$$\langle R_v \rangle_{pore} = \frac{N\pi\Delta\wp}{\tau} \left[\frac{R_0^4}{8\mu L} \int_0^\tau \sin^4\left(\frac{\pi t}{\tau} \right) dt + k_{3layer} R_0^2 \int_0^\tau \sin^2\left(\frac{\pi t}{\tau} \right) dt \right] \tag{D-4}$$

consider integral term of $\sin^4$ as follows

$$\int_0^\tau \sin^4\left(\frac{\pi t}{\tau} \right) dt = \int_0^\tau \left(\frac{1 - \cos(2\pi t/\tau)}{2} \right)^2 dt \tag{D-5}$$

$$= \frac{1}{4} \int_0^\tau \left(1 - 2\cos\left(\frac{2\pi t}{\tau} \right) + \cos^2\left(\frac{2\pi t}{\tau} \right) \right) dt$$

$$= \frac{1}{4} \int_0^\tau \left(1 - 2\cos\left(\frac{2\pi t}{\tau} \right) + \left(\frac{1 + \cos(4\pi t/\tau)}{2} \right) \right) dt$$

$$= \frac{1}{4} \int_0^\tau \left(\frac{3}{2} - 2\cos\left(\frac{2\pi t}{\tau} \right) + \frac{1}{2}\cos\left(\frac{4\pi t}{\tau} \right) \right) dt$$

$$= \frac{1}{4} \left[\frac{3}{2}\tau - \frac{\tau}{\pi}\left[\sin\left(\frac{2\pi t}{\tau} \right) \right]_0^\tau + \frac{\tau}{8\pi}\left[\sin\left(\frac{4\pi t}{\tau} \right) \right]_0^\tau \right]$$

$$= \frac{1}{4} \left[\frac{3}{2}\tau \right]$$

$$\int_0^\tau \sin^4\left(\frac{\pi t}{\tau} \right) dt = \frac{3}{8}\tau \tag{D-6}$$

and integral term of sine square as follows

$$\int_0^\tau \sin^2\left(\frac{\pi t}{\tau}\right) dt = \int_0^\tau \left(\frac{1-\cos(2\pi t/\tau)}{2}\right) dt \tag{D-7}$$

$$= \frac{1}{2} \int_0^\tau \left(1-\cos\left(\frac{2\pi t}{\tau}\right)\right) dt$$

$$= \frac{1}{2}\left[\tau - \frac{\tau}{2\pi}\left[\sin\left(\frac{2\pi t}{\tau}\right)\right]_0^\tau \right]$$

$$\int_0^\tau \sin^2\left(\frac{\pi t}{\tau}\right) dt = \frac{1}{2}\tau \tag{D-8}$$

substituting Eqs.(D-6) and (D-8) into Eq.(D-4), the average volume flow rate that R(t) is a sine function is

$$\langle R_v \rangle_{pore} = N\pi\Delta\wp\left[\frac{3}{64}\frac{R_0^4}{8\mu L} + \frac{1}{2}k_{3layer}R_0^2\right] \tag{D-9}$$

In case of R(t) as a cosine function, R(t) is expressed as

$$R = R_0 \cos\left(\frac{\pi t}{2\tau}\right) \tag{D-10}$$

substitutions of expression in Eq.(D-10) into Eq.(D-2) yield the following for the averaged volume flow rate that R(t) is cosine function.

$$\langle R_v \rangle_{pore} = \frac{N\pi\Delta\wp}{\tau}\left[\frac{R_0^4}{8\mu L}\int_0^\tau \cos^4\left(\frac{\pi t}{2\tau}\right) dt + k_{3layer}R_0^2\int_0^\tau \cos^2\left(\frac{\pi t}{2\tau}\right) dt\right] \tag{D-11}$$

consider integral term of $\cos^4$ as follows

$$\int_0^\tau \cos^4\left(\frac{\pi t}{2\tau}\right) dt = \int_0^\tau \left(\frac{1+\cos(2\pi t/2\tau)}{2}\right)^2 dt \tag{D-12}$$

$$= \frac{1}{4}\int_0^\tau \left(1+\cos\left(\frac{\pi t}{\tau}\right)\right)^2 dt$$

$$= \frac{1}{4}\int_0^\tau \left(1+2\cos\left(\frac{\pi t}{\tau}\right) + \cos^2\left(\frac{\pi t}{\tau}\right)\right) dt$$

$$= \frac{1}{4}\int_0^\tau \left(1+2\cos\left(\frac{\pi t}{\tau}\right) + \left(\frac{1+\cos(2\pi t/\tau)}{2}\right)\right) dt$$

$$= \frac{1}{4} \int_0^\tau \left(\frac{3}{2} + 2\cos\left(\frac{\pi t}{\tau}\right) + \frac{1}{2}\cos\left(\frac{2\pi t}{\tau}\right) \right) dt$$

$$= \frac{1}{4}\left[\frac{3}{2}\tau + \frac{2\tau}{\pi}\left[\sin\left(\frac{\pi t}{\tau}\right)\right]_0^\tau + \frac{\tau}{4\pi}\left[\sin\left(\frac{2\pi t}{\tau}\right)\right]_0^\tau \right]$$

$$= \frac{1}{4}\left[\frac{3}{2}\tau \right]$$

$$\int_0^\tau \cos^4\left(\frac{\pi t}{2\tau}\right) dt = \frac{3}{8}\tau \tag{D-13}$$

and integral term of sine square as follows

$$\int_0^\tau \cos^2\left(\frac{\pi t}{2\tau}\right) dt = \int_0^\tau \left(\frac{1 + \cos(2\pi t/2\tau)}{2} \right) dt \tag{D-14}$$

$$= \frac{1}{2}\int_0^\tau \left(1 + \cos\left(\frac{\pi t}{\tau}\right)\right) dt$$

$$= \frac{1}{2}\left[\tau + \frac{\tau}{\pi}\left[\sin\left(\frac{\pi t}{\tau}\right)\right]_0^\tau \right]$$

$$\int_0^\tau \cos^2\left(\frac{\pi t}{2\tau}\right) dt = \frac{1}{2}\tau \tag{D-15}$$

substituting Eqs.(D-13) and (D-15) into Eq.(D11), the average volume flow rate that R(t) as a cosine function is

$$\langle R_v \rangle_{pore} = N\pi\Delta\wp\left[\frac{3}{64}\frac{R_0^4}{8\mu L} + \frac{1}{2}k_{3layer}R_0^2 \right] \tag{D-16}$$

Eqs.(D-9) and (D-16) are the averaged volume flow rate of pore that R(t) are function of sine and cosine, respectively, are exactly the same.

Appendix E

Parameters for calculation in healthy human and patients with diabetic nephropathy

In healthy human

Table E-1 Parameters for calculation in healthy human.

parameters	quantities	parameters	quantities
SNGFR	1.04×10^{-12} m^3/s	k_{4layer}	6.37×10^{-10} m/s/Pa
S_{3layer}	2.90×10^{-7} m^2	$\Delta \wp$	41.34 mmHg
k_{3layer}	2.46×10^{-9} m/s/Pa	$\Delta \Pi$	31.48 mmHg
S_{4layer}	1.24×10^{-7} m^2		

In patients with diabetic nephropathy

Table E-2 Parameters for calculation in patients with diabetic nephropathy.

parameters	quantities	parameters	quantities
SNGFR	8.22×10^{-13} m^3/s	k_{4layer}	5.39×10^{-11} m/s/Pa
S_{3layer}	8.20×10^{-8} m^2	$\Delta \wp$	61.73 mmHg
k_{3layer}	2.10×10^{-9} m/s/Pa	$\Delta \Pi$	26.34 mmHg
S_{4layer}	3.51×10^{-8} m^2		